LA-UR-20-26036
Approved for public release; distribution is unlimited.

Title: Parallel Implicit Hydrodynamics for High Explosive Burn Calculations

Author(s): Scannapieco, Anthony J.
Chang, Chong

Intended for: Report

Issued: 2020-08-06

Parallel Implicit Hydrodynamics for High Explosive Burn Calculations

A. J. Scannapieco and C. H. Chang

August 8, 2020

Abstract

High explosives in hostile environments will require calculational capabilities that model processes, which evolve on timescales from minutes to nanoseconds. Eventually the HE will begin to move metal. To handle this temporal evolution an implicit hydrodynamics coupled to the chemical release of the HE energy is required. In addition, the use of chemical kinetics to model the transition from, the initially, slow heating of a confined high explosive through to deflagration and on to detonation requires many computational zones to model high explosive engineering systems. This requirement means that a fully parallel implicit hydrodynamics is essential. In this paper we present the calculation of a nonlinear matrix equation for the advanced particle pressure that has been made parallel and implemented in our AMR code, BABBO. This new parallel implicit hydrodynamics has been applied to a cookoff problem, as well as, one and two dimensional shock problems. Results are presented and discussed.

1 Introduction

The central issue in spanning the timescales we encounter in our HE calculations is to forgo the use of a Courant time step control in an explicit hydrodynamics. This issue has been known for many years and many methods have been proposed. The fundamental method to do this is to develop an implicit calculation of the advanced particle pressure derived from the conservation laws of mass, momentum and energy for the fluid[1]. The derivation is performed using a full advanced time step difference representation of the conservation laws, which produces a matrix equation for the advanced time pressure. It is also essential that the Equation-of-State for the fluid be completely general. Both analytic, as well as, tabular EOS capabilities have to be inherent in the solver. Because of the potentially massive calculations encountered, the implicit solver must run in parallel, on all of the machine architectures we use in our high explosives calculations. This requirement of parallelism has necessitated that the solver be cast as a matrix equation; albeit, a nonlinear matrix equation, which necessitates that an iterative solution of the matrix is used[2].

2 Operator Split Physics

Operator split physics is the sine qua non of multi-physics codes. Because of the multi-physics nature of the calculations we perform in our physics codes, it has become a standard procedure in the creation of these codes. This physics split procedure, which has been used in the development of our explicit hydrodynamics provides the ability to replace a simple EOS call to obtain the pressure, that requires a Courant time step control, with an iterative matrix solve for the advanced pressure that obviates the need for the Courant time step control. Either procedure to obtain the pressure can be used in the calculation of the momenta, PDV work, and subsequently the advection. It becomes necessary to change only one step in the hydrodynamics calculation. This fact also produces an ability to seamlessly transform from an implicit hydrodynamics to an explicit hydrodynamics during a calculation.

In a typical HE simulation the split is represented as follows.

- HE energy deposition
  - Arrhenius burn
  - Henson-Smilowitz chemical kinetics
- Hydrodynamics
  - Pressure acceleration
  - Adiabatic work from fluid compression and expansion
  - Viscous dissipation
  - Advection
- Thermal conduction
  - Implicit
  - Electron and ion

2.1 Full implicit Euler equations

The full implicit Euler equations are written using the advanced time step quantities on the left-hand side of the equations for the advancement of density, velocities and specific internal energy

$$\frac{d\rho}{d\tau} = -\rho^{n+1}\nabla \cdot \vec{v}^{n+1} \tag{1}$$

$$\frac{d\vec{v}}{d\tau} = -\frac{1}{\rho^{n+1}}\nabla P^{n+1} \tag{2}$$

$$\frac{de}{d\tau} = -\frac{P^{n+1}}{\rho^{n+1}}\nabla \cdot \vec{v}^{n+1} \tag{3}$$

where the total time derivative is

$$\frac{d}{d\tau} \equiv \frac{\partial}{\partial \tau} + \vec{v} \cdot \nabla \tag{4}$$

Substituting the finite difference representation of the time derivative in equations 1-3 yields a set of implicit finite difference equations that advance the density, specific internal energy and velocities from the n time step to the $n+1$ time step.

$$\frac{\rho^{n+1} - \rho^n}{\delta\tau} = -\rho^{n+1} \nabla \cdot \vec{v}^{n+1} \tag{5}$$

$$\rho^{n+1} = \frac{\rho^n}{(1 + \delta\tau \nabla \cdot \vec{v}^{n+1})} \tag{6}$$

$$\rho^{n+1} - \rho^n = -\rho^n \frac{\delta\tau \nabla \cdot \vec{v}^{n+1}}{(1 + \delta\tau \nabla \cdot \vec{v}^{n+1})} \tag{7}$$

$$\frac{\vec{v}^{n+1} - \vec{v}^n}{\delta\tau} = -\frac{1}{\rho^{n+1}} \nabla P^{n+1} \tag{8}$$

$$\vec{v}^{n+1} = \vec{v}^n - \frac{\delta\tau}{\rho^{n+1}} \nabla P^{n+1} \tag{9}$$

$$\frac{e^{n+1} - e^n}{\delta\tau} = -\frac{P^{n+1}}{\rho^{n+1}} \nabla \cdot \vec{v}^{n+1} \tag{10}$$

$$e^{n+1} = e^n - \frac{P^{n+1}}{\rho^{n+1}} \delta\tau \nabla \cdot \vec{v}^{n+1} \tag{11}$$

3 Calculation of the matrix equation for P^{n+1}

To begin the calculation of the implicit matrix equation for the advanced pressure take the divergence of equation 9

$$\nabla \cdot \vec{v}^{n+1} = \nabla \cdot \vec{v}^{n} - \nabla \left(\frac{\delta\tau}{\rho^{n+1}} \right) \cdot \nabla P^{n+1} - \left(\frac{\delta\tau}{\rho^{n+1}} \right) \nabla^2 P^{n+1} \tag{12}$$

From equation 6 write $\nabla \left(\frac{\delta\tau}{\rho^{n+1}} \right)$ as

$$\nabla \left(\frac{\delta\tau(1+\delta\tau\nabla\cdot\vec{v}^{n+1})}{\rho^{n}} \right) = -\frac{\delta\tau(1+\delta\tau\nabla\cdot\vec{v}^{n+1})}{(\rho^{n})^2}\nabla\rho^{n} + \frac{\delta\tau^2}{\rho^{n}}\nabla(\nabla\cdot\vec{v}^{n+1}) \tag{13}$$

or

$$\nabla \left(\frac{\delta\tau}{\rho^{n+1}} \right) = -\frac{\delta\tau}{(\rho^{n})^2}\nabla\rho^{n} - \frac{\delta\tau^2}{(\rho^{n})^2}\nabla\rho^{n}(\nabla\cdot\vec{v}^{n+1}) - \frac{\delta\tau^2}{\rho^{n}}\nabla(\nabla\cdot\vec{v}^{n+1}) \tag{14}$$

Next write $\nabla \cdot \vec{v}^{n+1}$ to first order in $\delta\tau$ as

$$\nabla \cdot \vec{v}^{n+1} \simeq \nabla \cdot \vec{v}^{n} + \frac{\delta\tau}{(\rho^{n})^2}\nabla\rho^{n} \cdot \nabla P^{n+1} - \frac{\delta\tau}{\rho^{n}}\nabla^2 P^{n+1} \tag{15}$$

If the Equation-Of-State is of the form $P = \Psi(\rho, e)$, then at the $n+1$ time step

$$P^{n+1} = \Psi(\rho^{n+1}, e^{n+1}) \tag{16}$$

Taylor series expanding about the n time step gives

$$P^{n+1} \simeq P^{n} + \left.\frac{\partial\Psi}{\partial\rho}\right|_{n} (\rho^{n+1} - \rho^{n}) + \left.\frac{\partial\Psi}{\partial e}\right|_{n} (e^{n+1} - e^{n}) \tag{17}$$

Substituting the equations for ρ^{n+1} and e^{n+1} obtain

$$\begin{aligned} P^{n+1} \simeq P^{n} &- \left.\frac{\partial\Psi}{\partial\rho}\right|_{n} \frac{\delta\tau\rho^{n}\nabla\cdot\vec{v}^{n+1}}{(1+\delta\tau\nabla\cdot\vec{v}^{n+1})} \\ &- \left.\frac{\partial\Psi}{\partial e}\right|_{n} \frac{(1+\delta\tau\nabla\cdot\vec{v}^{n+1})}{\rho^{n}}\delta\tau P^{n+1}\nabla\cdot\vec{v}^{n+1} \end{aligned} \tag{18}$$

Defining, $D^{i} \equiv \nabla \cdot \vec{v}^{i}$, equation 18 can be written as

$$\begin{aligned} P^{n+1}(1+\delta\tau D^{n+1}) = P^n(1+\delta\tau D^{n+1}) &- \left.\frac{\partial\Psi}{\partial\rho}\right|_n \delta\tau\rho^n D^{n+1} \\ &- \left.\frac{\partial\Psi}{\partial e}\right|_n \delta\tau\frac{D^{n+1}}{\rho^n}P^{n+1} \\ &- \left.\frac{\partial\Psi}{\partial e}\right|_n 2\frac{(\delta\tau D^{n+1})^2}{\rho^n}P^{n+1} \\ &- \left.\frac{\partial\Psi}{\partial e}\right|_n \frac{(\delta\tau D^{n+1})^3}{\rho^n}P^{n+1} \end{aligned} \tag{19}$$

Equation 15 can also be rewritten as

$$D^{n+1} \simeq D^n + \frac{\delta\tau}{(\rho^n)^2}\nabla\rho^n \cdot \nabla P^{n+1} - \frac{\delta\tau}{\rho^n}\nabla^2 P^{n+1} \tag{20}$$

Approximating $\delta\tau D^{n+1}$ to order $\delta\tau^2$, yields

$$(\delta\tau D^{n+1})^1 \simeq \delta\tau D^n + \frac{\delta\tau^2}{(\rho^n)^2}\nabla\rho^n \cdot \nabla P^{n+1} - \frac{\delta\tau^2}{\rho^n}\nabla^2 P^{n+1} \tag{21}$$

$$(\delta\tau D^{n+1})^2 \simeq (\delta\tau D^n)^2 \tag{22}$$

$$(\delta\tau D^{n+1})^3 \simeq 0 \tag{23}$$

Therefore equation 19 becomes

$$\begin{aligned} P^{n+1}(1+\delta\tau D^{n+1}) = P^n(1+\delta\tau D^{n+1}) &- \left.\frac{\partial\Psi}{\partial\rho}\right|_n \delta\tau\rho^n D^{n+1} \\ &- \left.\frac{\partial\Psi}{\partial e}\right|_n \delta\tau\frac{D^{n+1}}{\rho^n}P^{n+1} \\ &- \left.\frac{\partial\Psi}{\partial e}\right|_n 2\frac{(\delta\tau D^n)^2}{\rho^n}P^{n+1} \end{aligned} \tag{24}$$

Finally, substituting equation 20 into equation 24 and after some manipulation the non-linear matrix equation for the advanced time pressure, P^{n+1} is

$$
\begin{aligned}
&-\frac{\delta\tau^2}{\rho^n}\left[P^{n+1}-P^n+\left.\frac{\partial\Psi}{\partial\rho}\right|_n\rho^n+\left.\frac{\partial\Psi}{\partial e}\right|_n\frac{P^{n+1}}{\rho^n}\right]\nabla^2P^{n+1}\\
&+\frac{\delta\tau^2}{\rho^n}\left[P^{n+1}-P^n+\left.\frac{\partial\Psi}{\partial\rho}\right|_n\rho^n+\left.\frac{\partial\Psi}{\partial e}\right|_n\frac{P^{n+1}}{\rho^n}\right]\frac{\nabla\rho^n}{\rho^n}\cdot\nabla P^{n+1}\\
&+\left[(1+\delta\tau D^n)+\left.\frac{\partial\Psi}{\partial e}\right|_n\frac{\delta\tau}{\rho^n}D^n+\left.\frac{\partial\Psi}{\partial e}\right|_n\frac{2}{\rho^n}(\delta\tau D^n)^2\right]P^{n+1}=\\
&\left[P^n(1+\delta\tau D^n)-\left.\frac{\partial\Psi}{\partial\rho}\right|_n\rho^n\delta\tau D^n\right]
\end{aligned}
\tag{25}
$$

3.1 Iteration procedure

Because of the non-linear nature of the matrix, equation 25 must be solved by iteration. To do this, rewrite equation 25 as the $\nu+1$ iterate of that equation.

$$
\begin{aligned}
&-\frac{\delta\tau^2}{\rho^n}\left[P^{\nu+1}-P^n+\left.\frac{\partial\Psi}{\partial\rho}\right|_n\rho^n+\left.\frac{\partial\Psi}{\partial e}\right|_n\frac{P^{\nu+1}}{\rho^n}\right]\nabla^2P^{\nu+1}\\
&+\frac{\delta\tau^2}{\rho^n}\left[P^{\nu+1}-P^n+\left.\frac{\partial\Psi}{\partial\rho}\right|_n\rho^n+\left.\frac{\partial\Psi}{\partial e}\right|_n\frac{P^{\nu+1}}{\rho^n}\right]\frac{\nabla\rho^n}{\rho^n}\cdot\nabla P^{\nu+1}\\
&+\left[(1+\delta\tau D^n)+\left.\frac{\partial\Psi}{\partial e}\right|_n\frac{\delta\tau}{\rho^n}D^n+\left.\frac{\partial\Psi}{\partial e}\right|_n\frac{2}{\rho^n}(\delta\tau D^n)^2\right]P^{\nu+1}=\\
&\left[P^n(1+\delta\tau D^n)-\left.\frac{\partial\Psi}{\partial\rho}\right|_n\rho^n\delta\tau D^n\right]
\end{aligned}
\tag{26}
$$

To begin the iterations the $P^{\nu+1}$ terms in the matrix coefficients of the $\nabla^2P^{\nu+1}$ term and the $\nabla\rho^n\cdot\nabla P^{\nu+1}$ term are replaced by P^ν and the matrix is solved. The initial guess is $P^\nu=P^n$. Successive substitutions are performed until the pressures converge to a solution, or when $\mid P^{\nu+1}-P^\nu\mid/P^{\nu+1}<\varepsilon$, where $\varepsilon<<1$.

3.2 Gamma law gas EOS

If the equation of state is of the form

$$P=\Psi(\rho,e)=(\gamma-1)\rho e \tag{27}$$

then

$$\left.\frac{\partial \Psi}{\partial \rho}\right|_n = (\gamma - 1)e^n \tag{28}$$

$$\left.\frac{\partial \Psi}{\partial e}\right|_n = (\gamma - 1)\rho^n \tag{29}$$

and equation 25 becomes

$$\begin{aligned} &- \frac{\delta\tau^2}{\rho^n}\left[\gamma P^{n+1}\right]\nabla^2 P^{n+1} \\ &+ \frac{\delta\tau^2}{\rho^n}\left[\gamma P^{n+1}\right]\frac{\nabla\rho^n}{\rho^n}\cdot\nabla P^{n+1} \\ &+ \left[1 + \gamma\delta\tau D^n + 2(\gamma-1)(\delta\tau D^n)^2\right]P^{n+1} = \\ &+ P^n \end{aligned} \tag{30}$$

Equation 30 is the actual equation that is solved for the γ law gas shock problems in this report.

4 Time step controls

Time step controls are imposed on the implicit hydrodynamics to ensure accuracy in the calculation. The dominant controls that are relevant to the evolution of high explosives are the energy and pressure changes fractions per time step. The energy change time step control is critical when running with an Arrhenius or Henson-Smilowitz HE energy production source. The Courant condition is not employed in the implicit hydrodynamics. An advection velocity time step control is used to ensure that a variable is not advected by more than half a zone size in a time step. When the velocity is very small the overall time step can still be much larger than the Courant time step. In addition, when the minimum time step is less than a factor (greater than one) of the Courant time step the hydrodynamics can switch to the standard explicit code hydrodynamics. If multi-species physics is required only when near shock or shock conditions are realized this switch capability gives us the immediate ability to utilize the multi-species capabilities associated with the explicit hydrodynamics. As will be discussed in the summary section below, the multi-species parallel implicit hydrodynamics is the next step in our development of the implicit hydrodynamics.

5 Calculational results

Figures 1-2 show the results of a calculation of a planar shock tube with two γ law gas materials each with $\gamma = 1.4$, run with three AMR levels using the parallel implicit hydrodynamics. The smallest zone size in the calculation is $0.125\,\mu m$.

Figures 3-13 show the results of two calculations of the single level Frank-Kamenetskii problem for HMX run with and without the parallel implicit hydrodynamics. In each case a constant temperature of $220°C$ was imposed on the outer boundary of the problem and a zone size of $0.0002\,\mu m$ was used. Figure 4, in this series shows the time step as a function of cycle. At 1634 cycles the energy deposition from the Arrhenius burn becomes large and the time steps adjust accordingly. Figures 5-13 show the specific internal energy, burn fraction and velocity just before and just after the explosive onset of the energy deposition from the Arrhenius burn for the Frank-Kamenetskii problem run without (FK) and with (FK-IMPH) the parallel implicit hydrodynamics. For each variable in the Frank-Kamenetskii problem run with the parallel implicit hydrodynamics a later time in the calculation is also included.

Figures 14-27 show the results of a two-dimensional calculation of a two-material spherical shock problem run with the explicit and the parallel implicit hydrodynamics on sixteen processors, on a single AMR level with a zone size of $0.125\,\mu m$. The two materials are both γ law gasses with $\gamma = 1.4$. The material densities and specific internal energies are $\rho_1 = 1.00 \times 10^{-3}\,\mathrm{g/cc}$, $\rho_2 = 2.00 \times 10^{-4}\,\mathrm{g/cc}$, $e_1 = 2.5182 \times 10^{21}\,\mathrm{erg/g}$ and $e_2 = 2.5182 \times 10^{21}\,\mathrm{erg/g}$. What is displayed are contour plots of density, Mach number and specific internal energy for the explicit and implicit calculations at two different times. In Figure 27 there is a pronounced structure along the 45° line, which is due to the fact that an elliptic equation is being solved for the advanced pressure and the signal propagation speed is infinite. What is observed are the effects of the boundary conditions on the solution.

Figures 28-34 show the results of a two-dimensional calculation of a two-material shock problem using the parallel implicit hydrodynamics run with four AMR levels on sixteen processors. The smallest zone size in the calculation is $0.125\,\mu m$. The initial setup of densities and specific internal energies is identical to the single level two-dimensional shock problem. These results are presented to demonstrate the ability of the parallel implicit hydrodynamics to run with multiple AMR mesh levels on multiple processors.

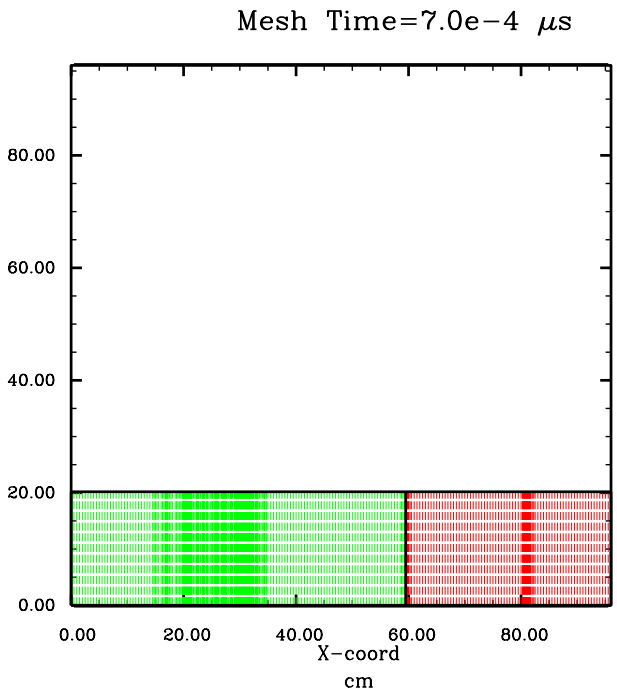

Figure 1: IMPH AMR mesh at $7.0 \times 10^{-4} \mu s$.

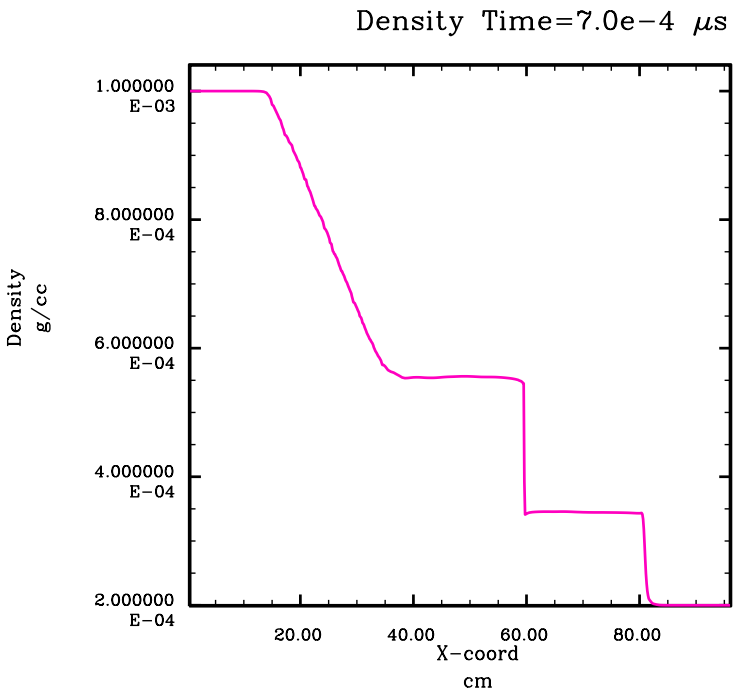

Figure 2: IMPH AMR shock density at $7.0 \times 10^{-4} \mu s$.

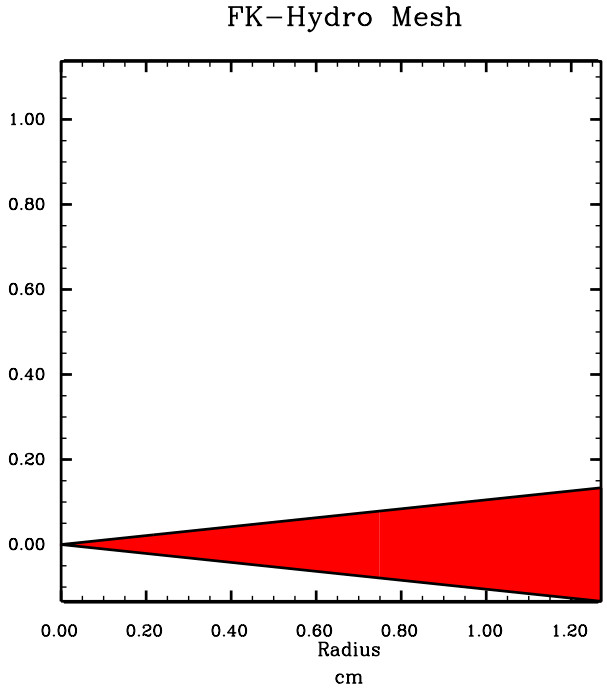

Figure 3: FK initial mesh HMX with 220° Celsius surface temperature.

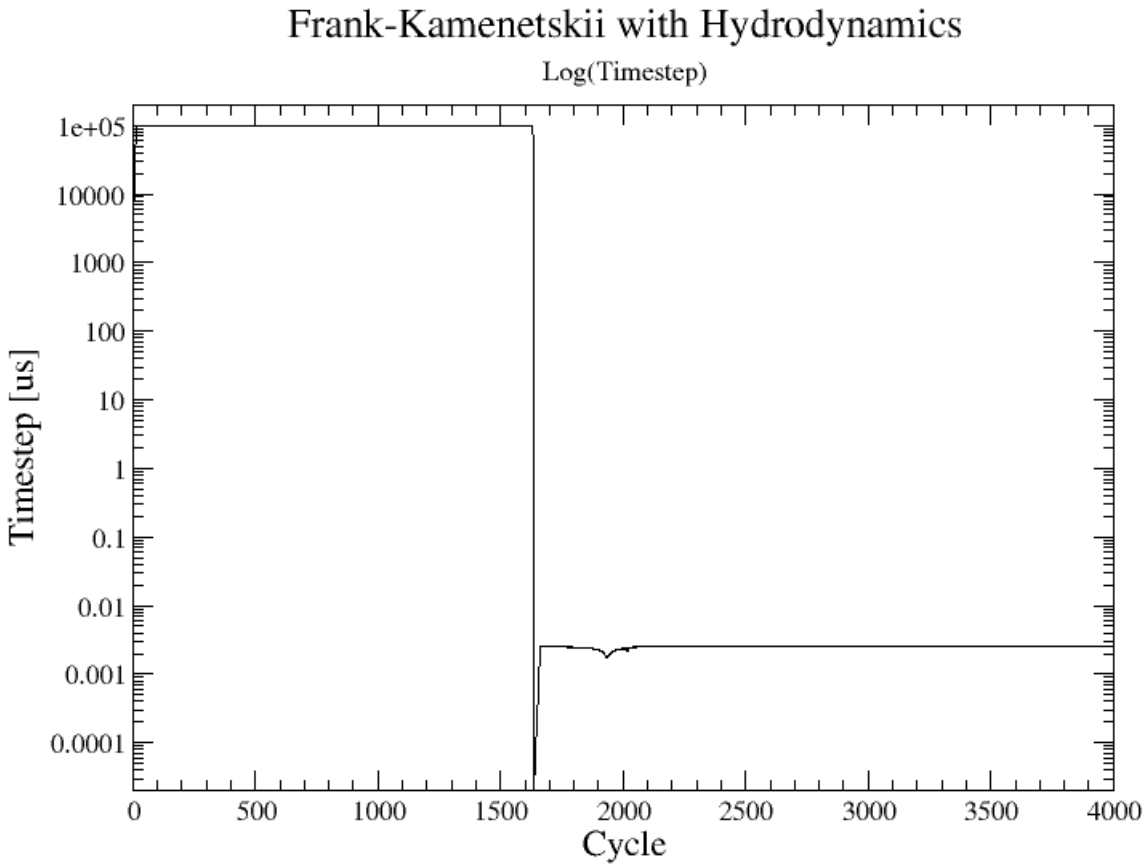

Figure 4: FK-IMPH time step vs cycle.

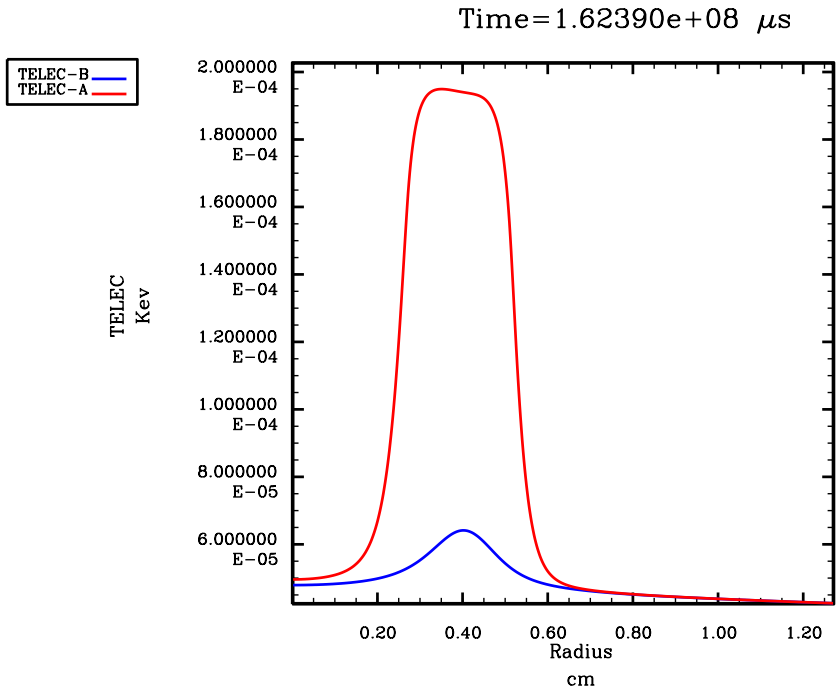

Figure 5: FK Electron temperature before and after $1.62390 \times 10^8 \mu s$.

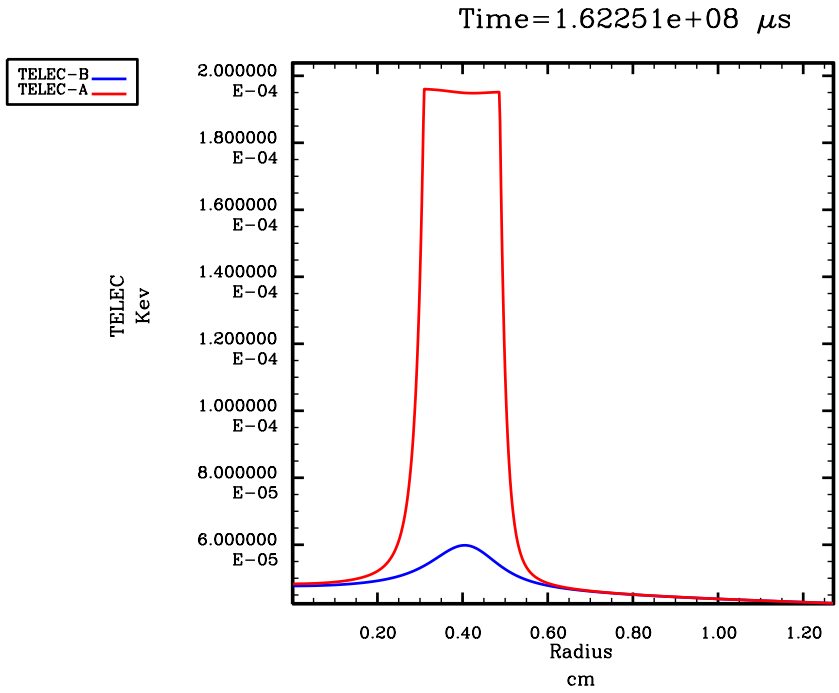

Figure 6: FK-IMPH Electron temperature before and after $1.62251 \times 10^8 \mu s$.

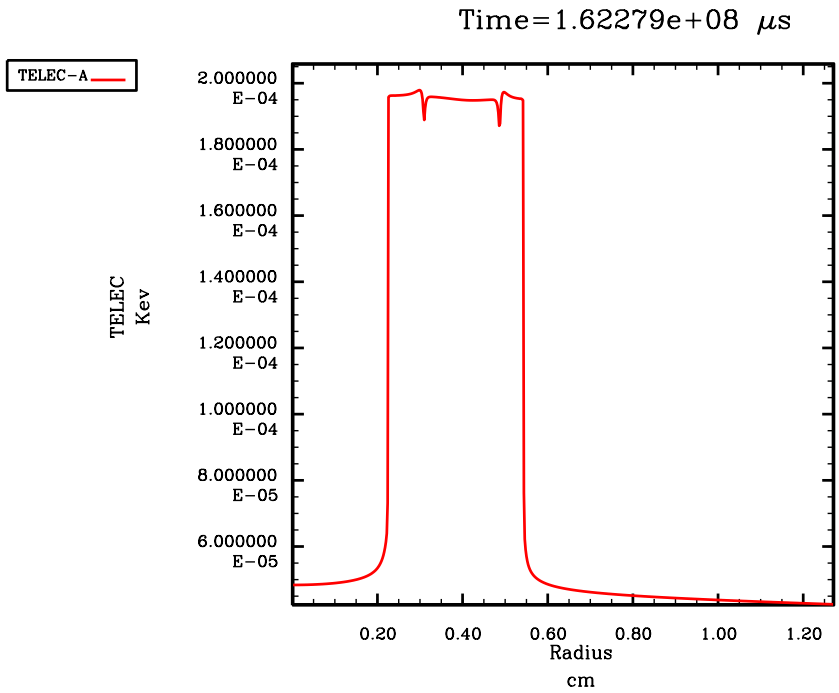

Figure 7: FK-IMPH Electron temperature at $1.62279 \times 10^8 \mu s$.

Figure 7 is a plot of the electron temperature at a time $2.8 \times 10^4\,\mu$s after the explosive onset of the HE energy deposition. The higher temperatures on the sides of the central peak are created by the shocks emanating from the region of the initial energy burst. The central peak corresponds to the peak in Figure 6.

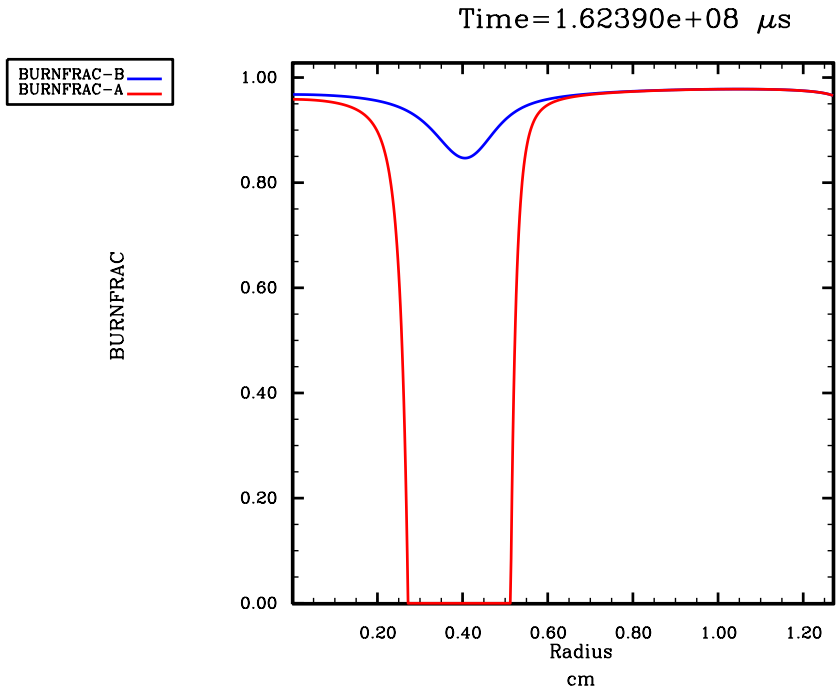

Figure 8: FK Burn fraction before and after $1.62390 \times 10^8 \mu s$.

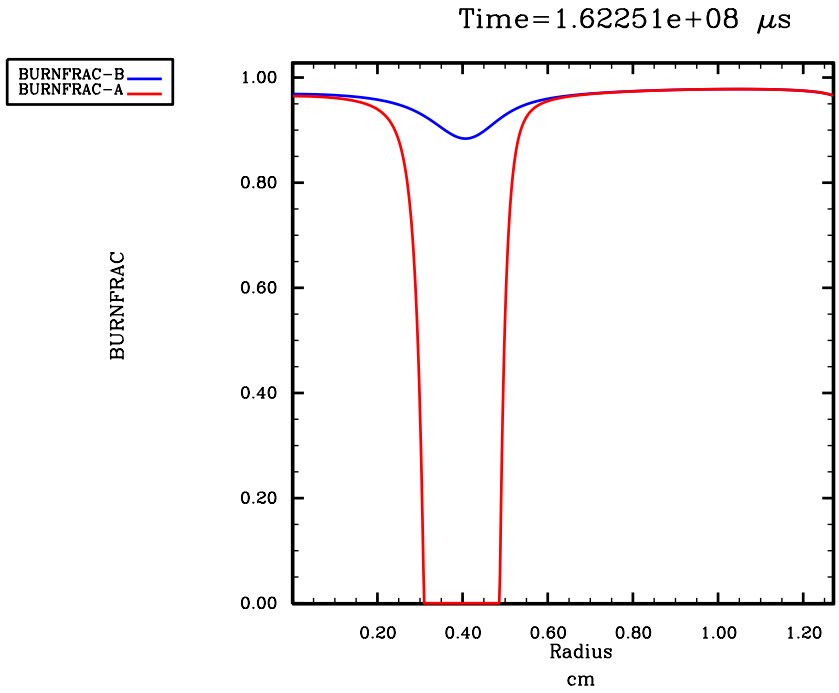

Figure 9: FK-IMPH Burn fraction before and after $1.62251 \times 10^8 \mu s$.

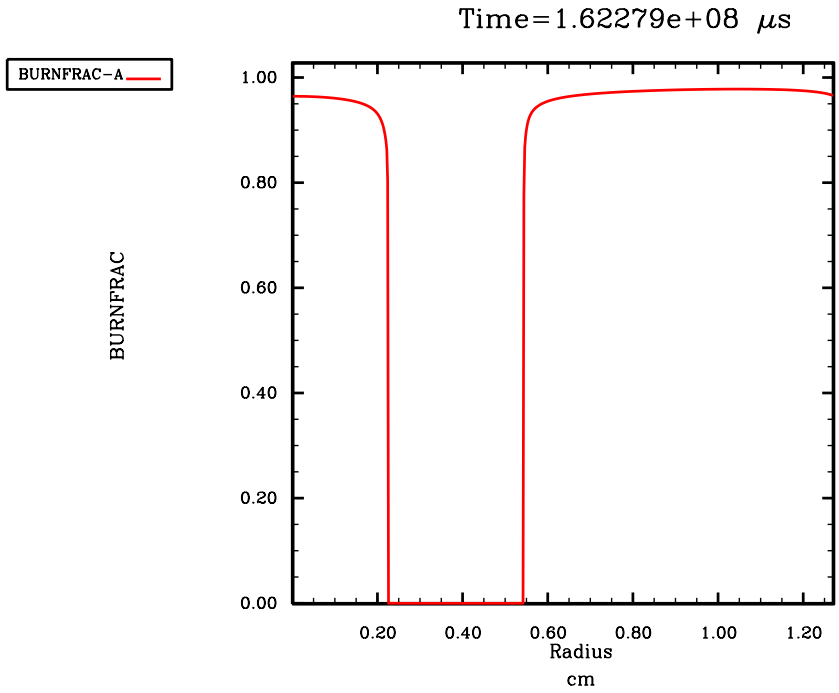

Figure 10: FK-IMPH Burn fraction at $1.62279 \times 10^8 \mu s$.

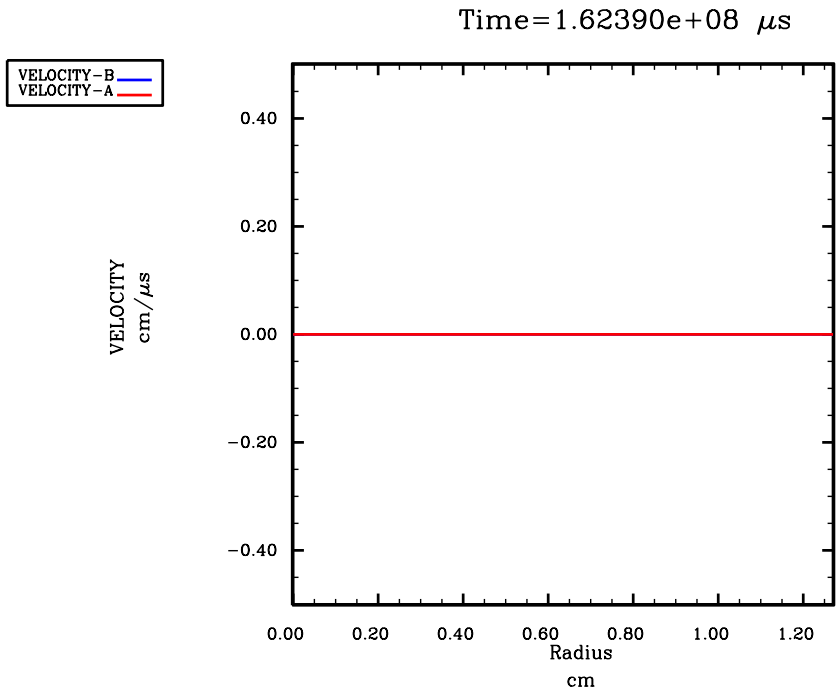

Figure 11: FK HE velocity before and after $1.62390 \times 10^8 \mu s$.

Figure 11 is a plot of the velocity at a time just before and just after the explosive onset of the HE energy deposition for the original Frank-Kamenetskii problem. Of course, the velocity is zero before and after, since the original Frank-Kamenetskii problem is run with Arrhenius burn, electron and ion thermal conduction and *no* hydrodynamics.

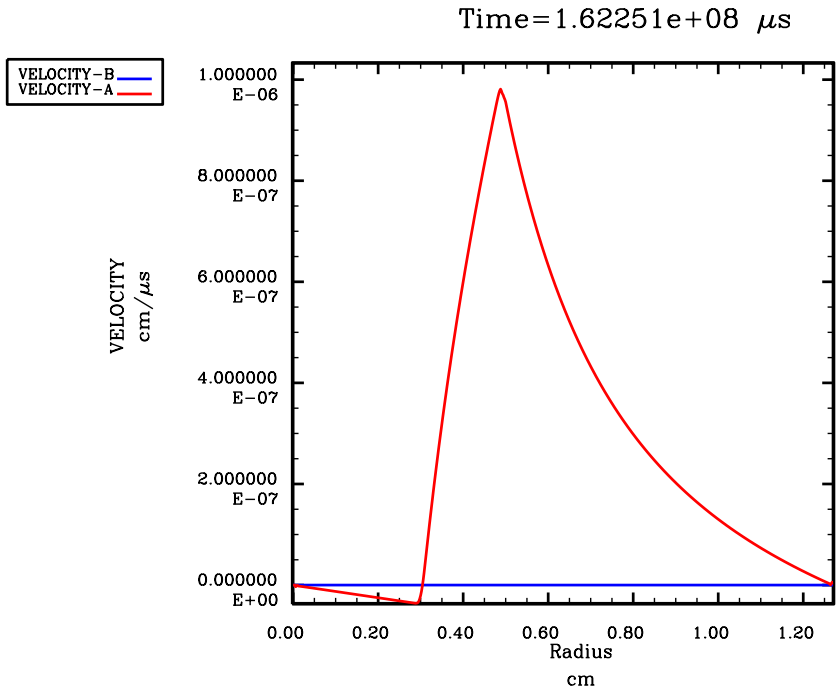

Figure 12: FK-IMPH HE velocity before and after $1.62251 \times 10^8 \mu s$.

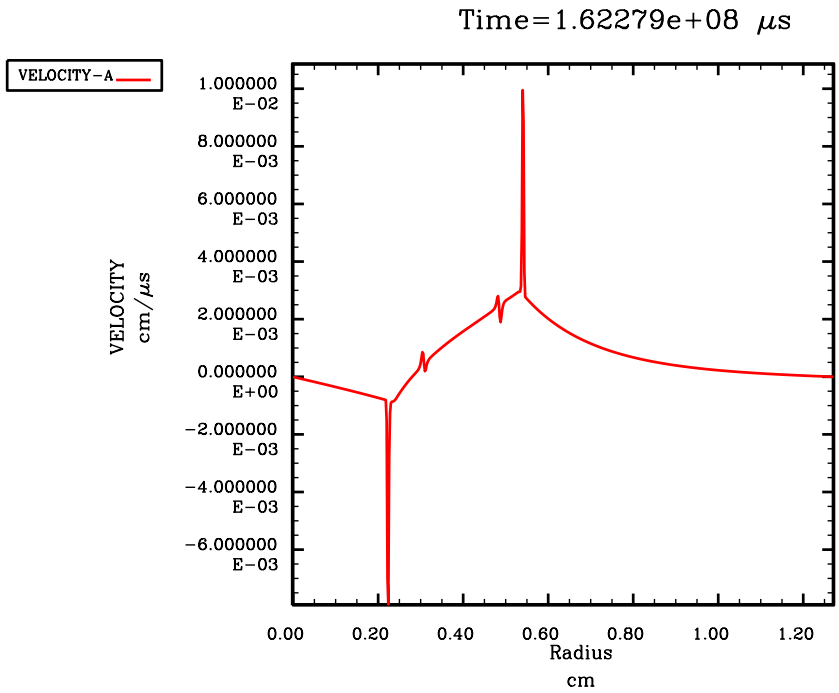

Figure 13: FK-IMPH HE velocity at $1.62279 \times 10^8 \mu s$.

Figure 13 is a plot of the velocity at a time $2.8 \times 10^4\,\mu$s after the explosive onset of the HE energy deposition. The small oscillations in the plot mirrors the drive from the initial onset of the velocity just after the burst of energy for the HE. The larger spikes represent the shocks emanating from the region of the initial energy burst.

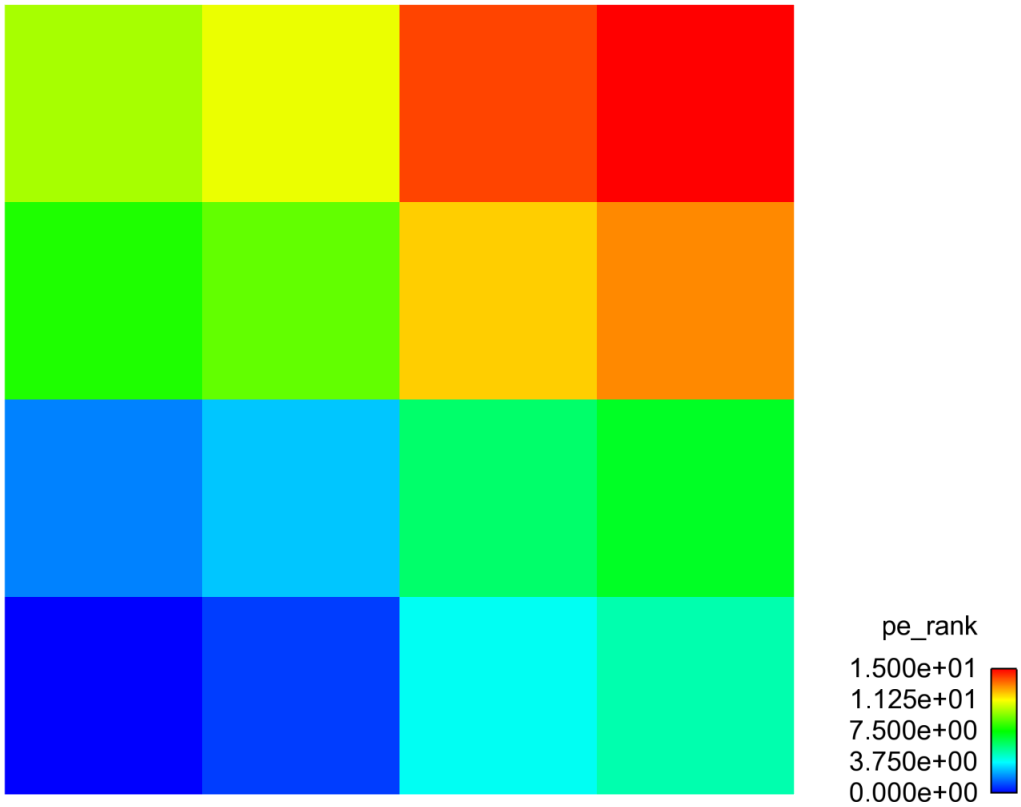

Figure 14: Explicit calculation processor map.

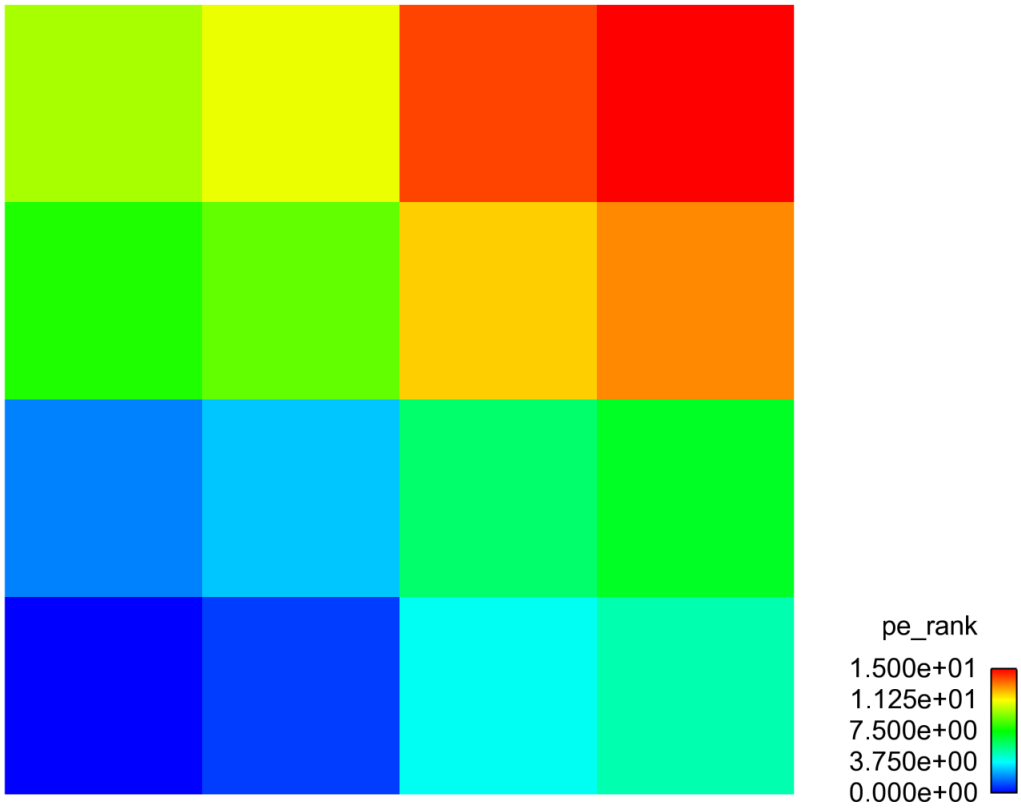

Figure 15: Implicit calculation processor map.

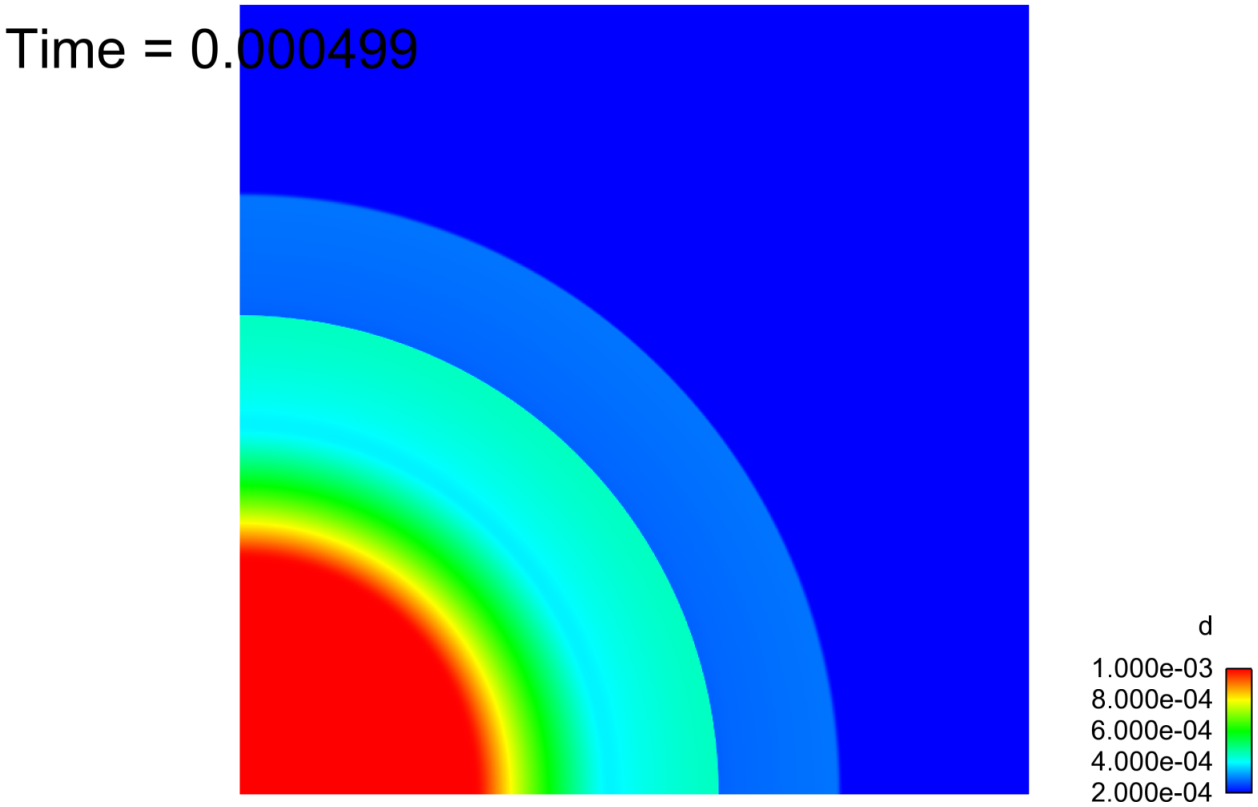

Figure 16: Explicit material density.

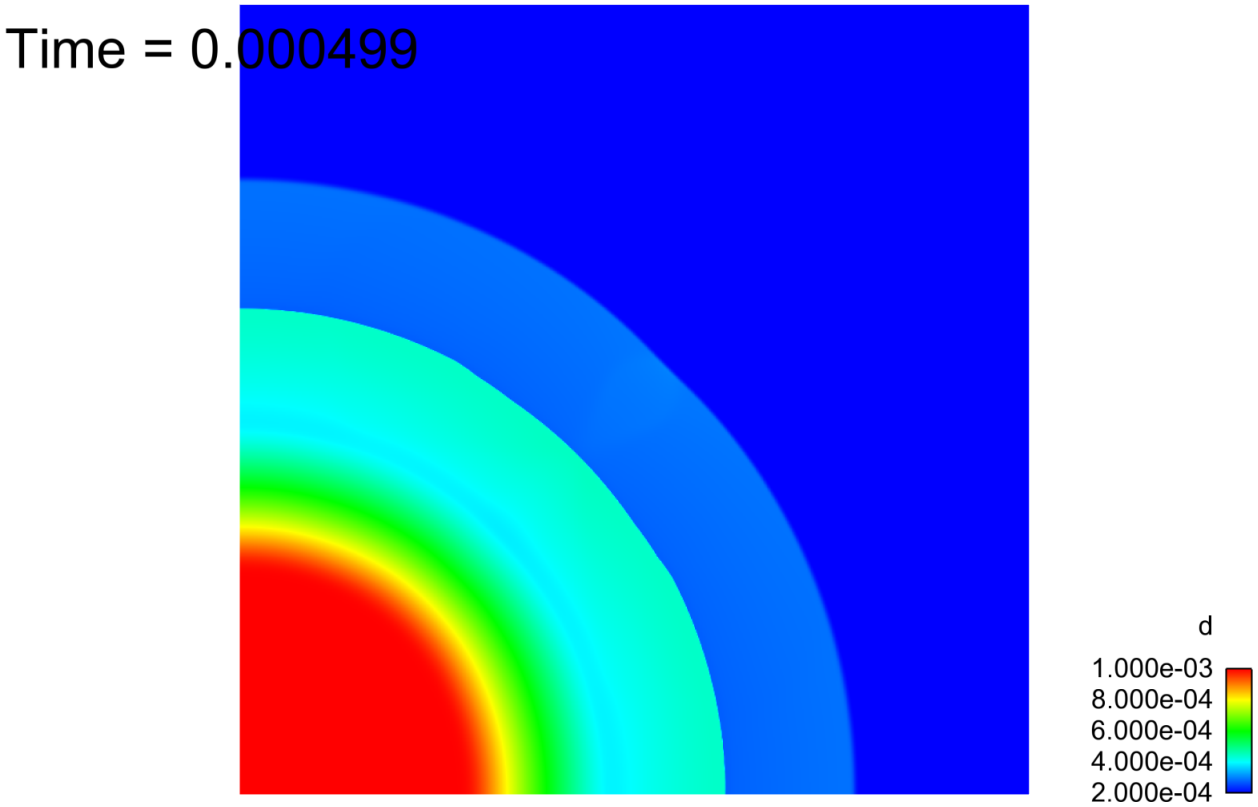

Figure 17: Implicit material density.

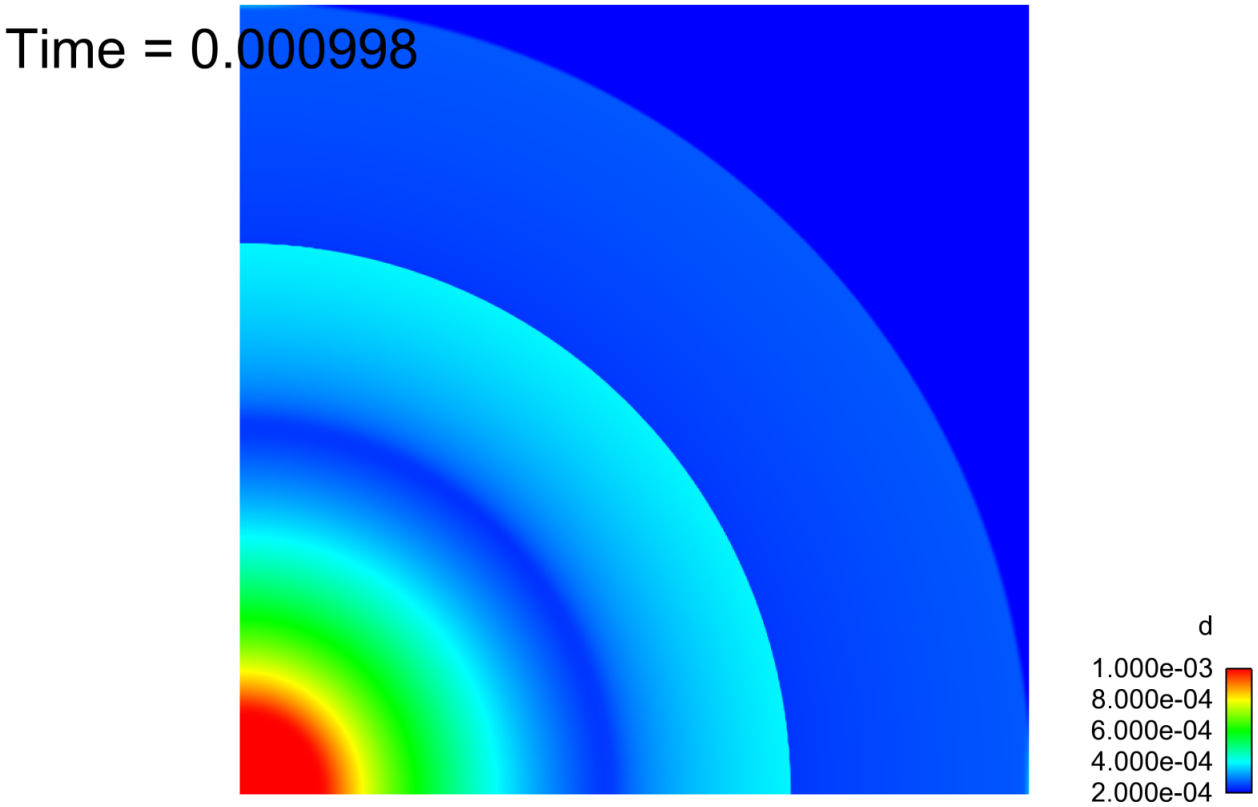

Figure 18: Explicit material density.

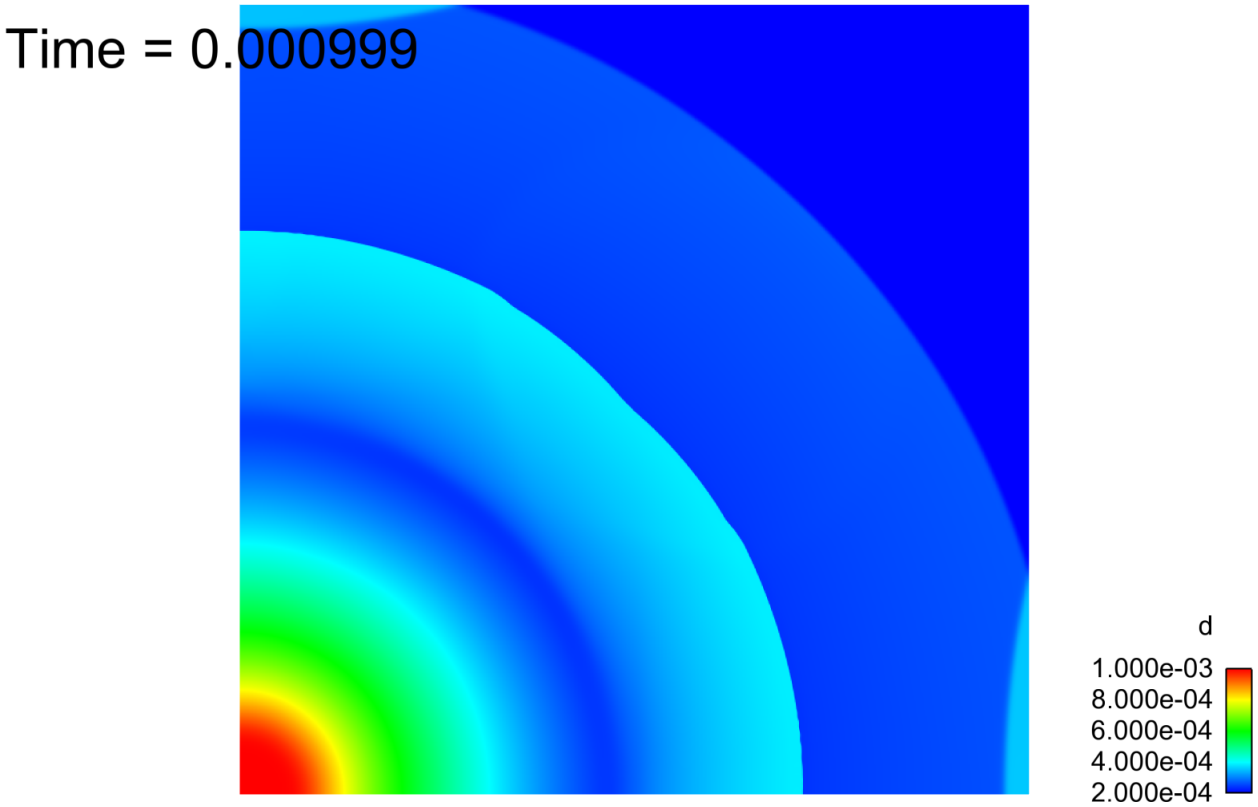

Figure 19: Implicit material density.

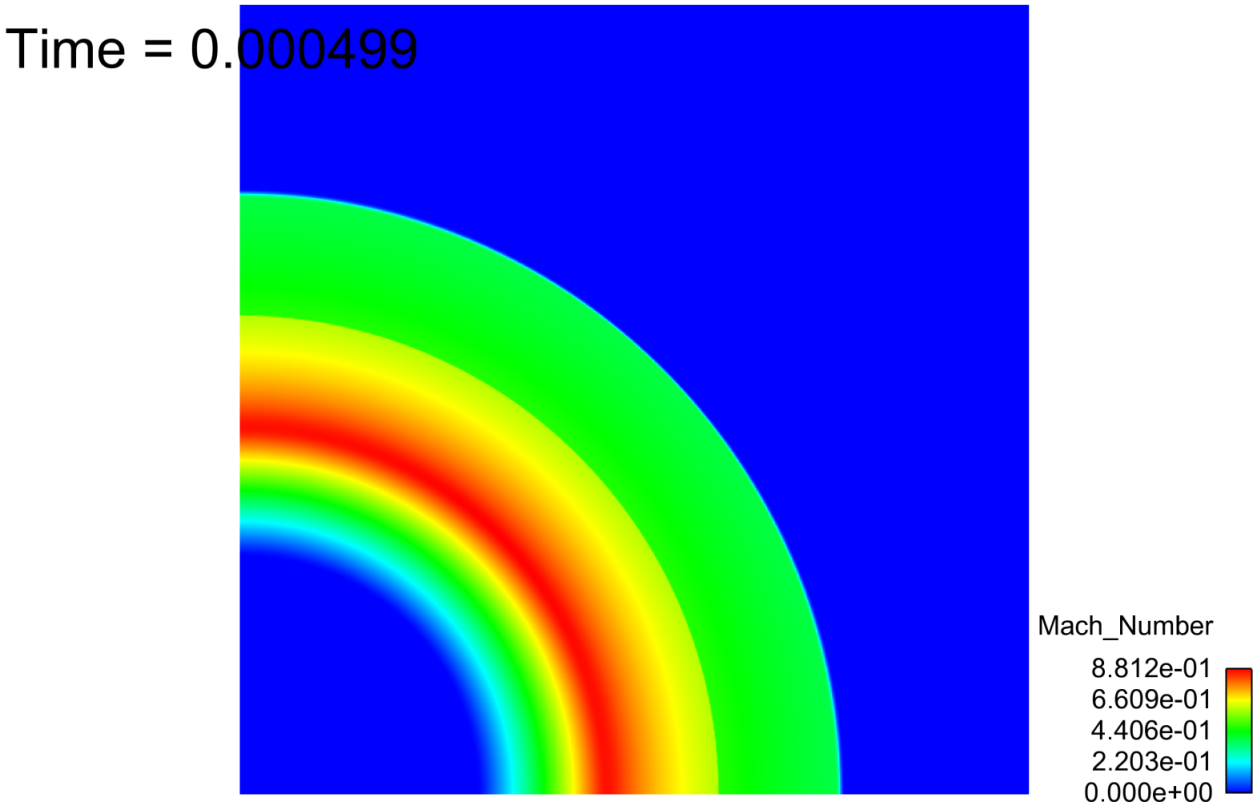

Figure 20: Explicit Mach number.

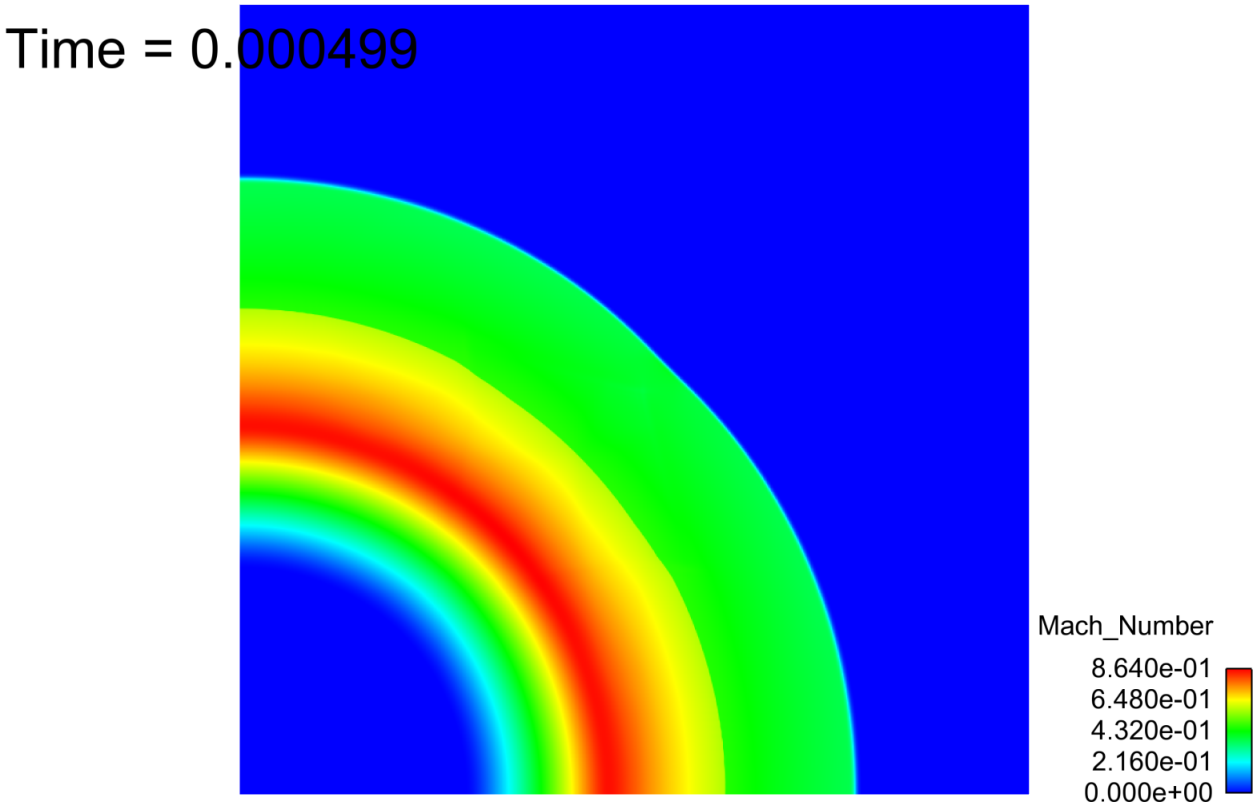

Figure 21: Implicit Mach number.

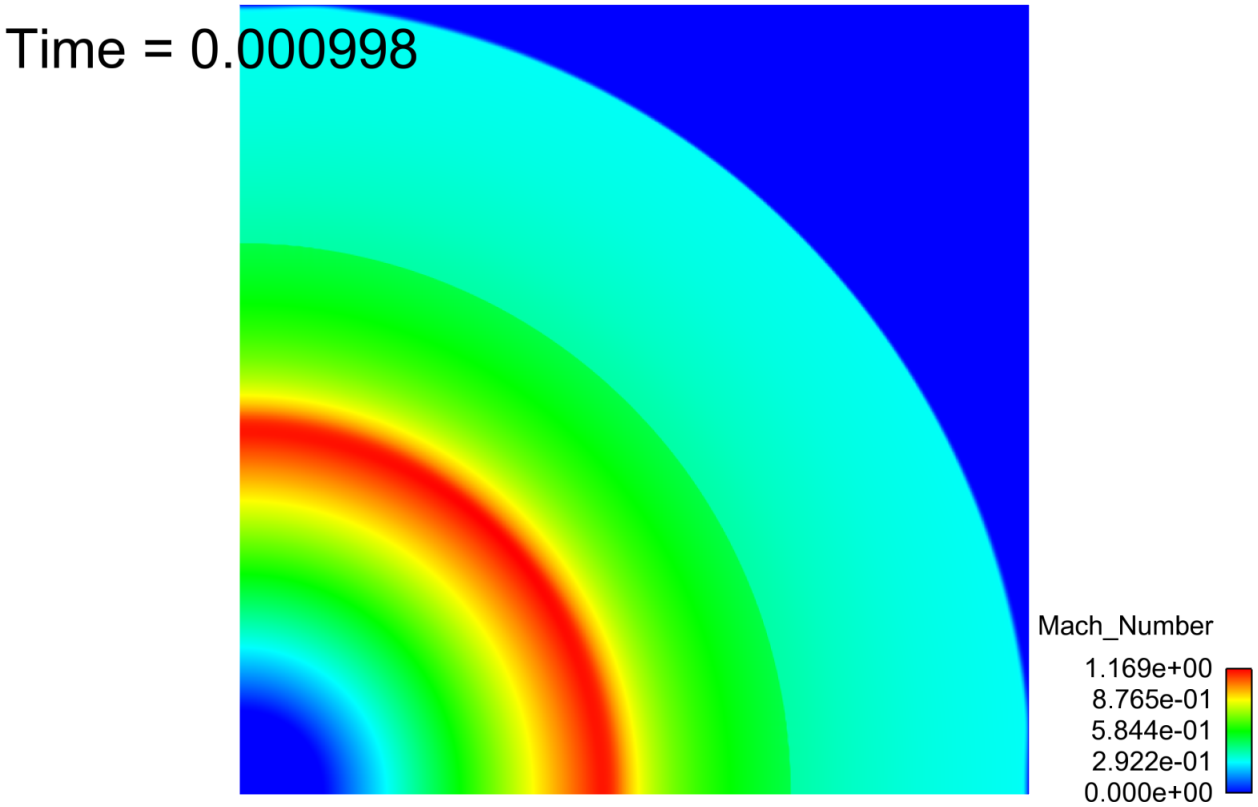

Figure 22: Explicit Mach number.

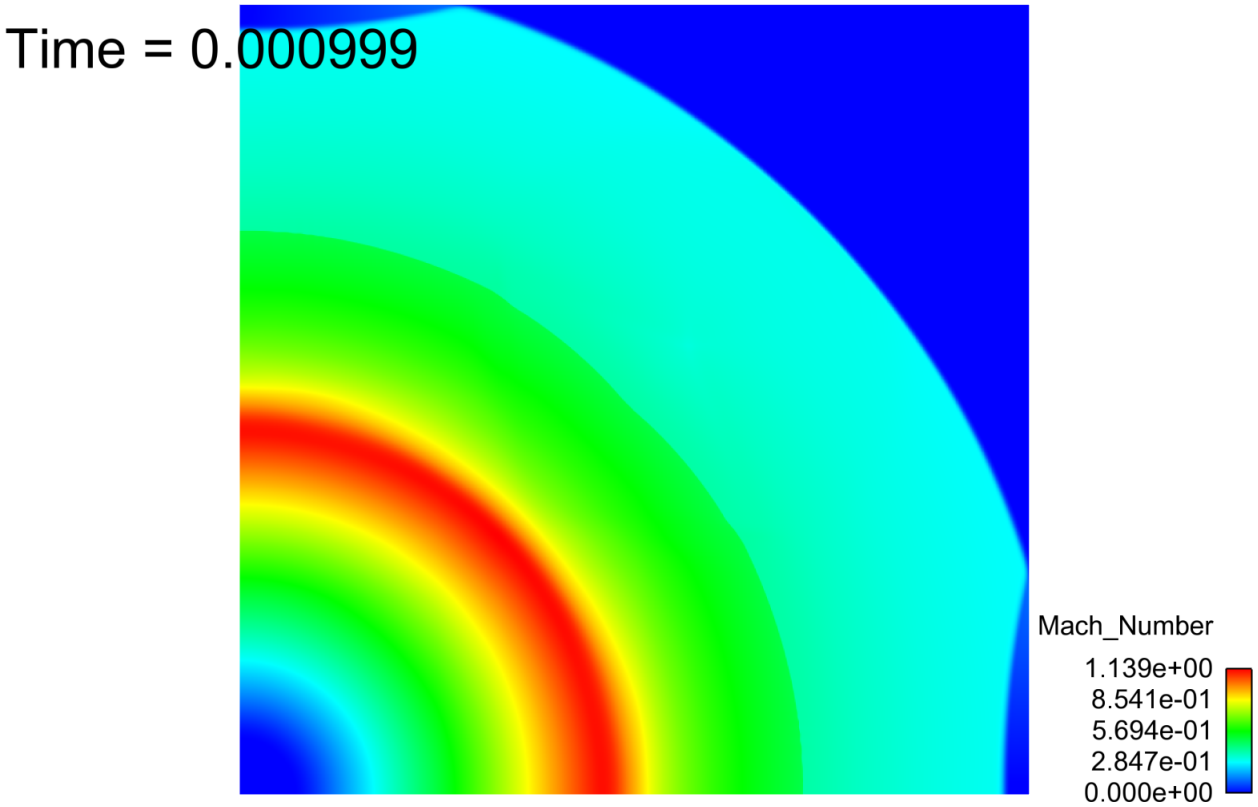

Figure 23: Implicit Mach number.

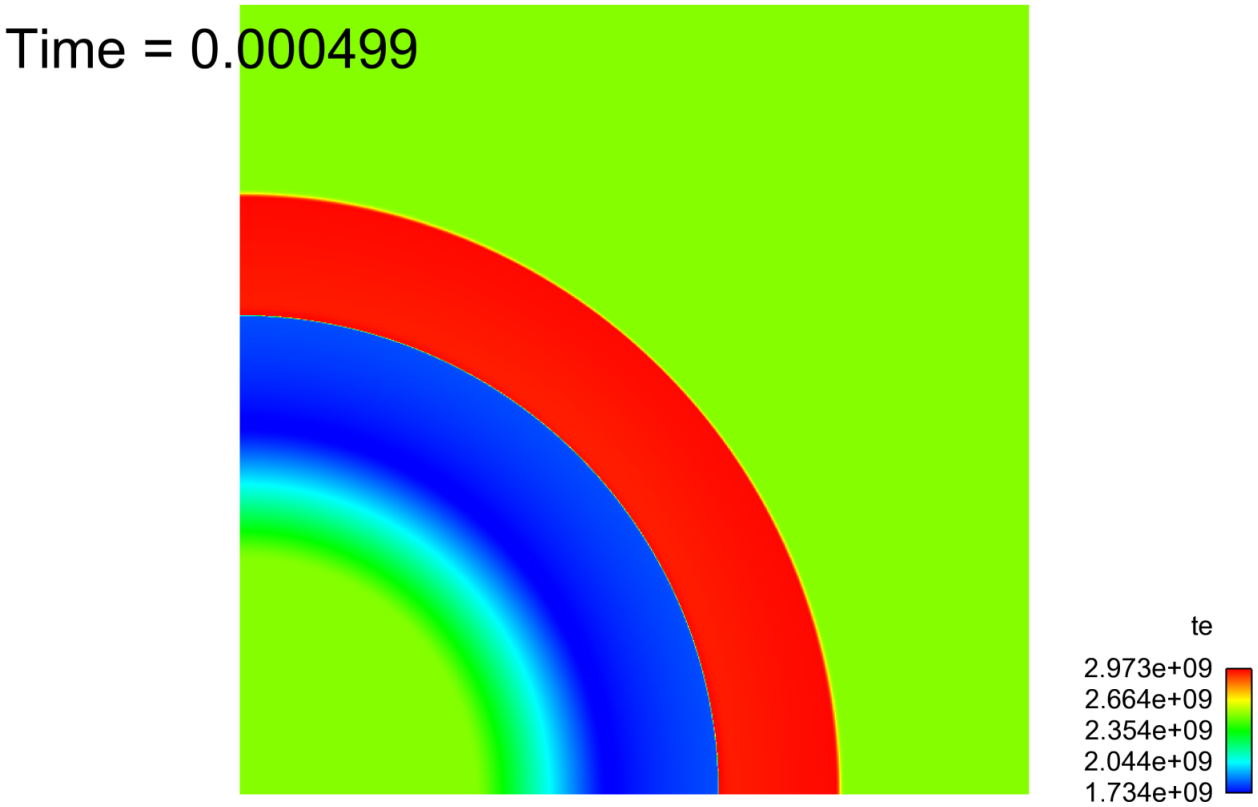

Figure 24: Explicit specific internal energy density.

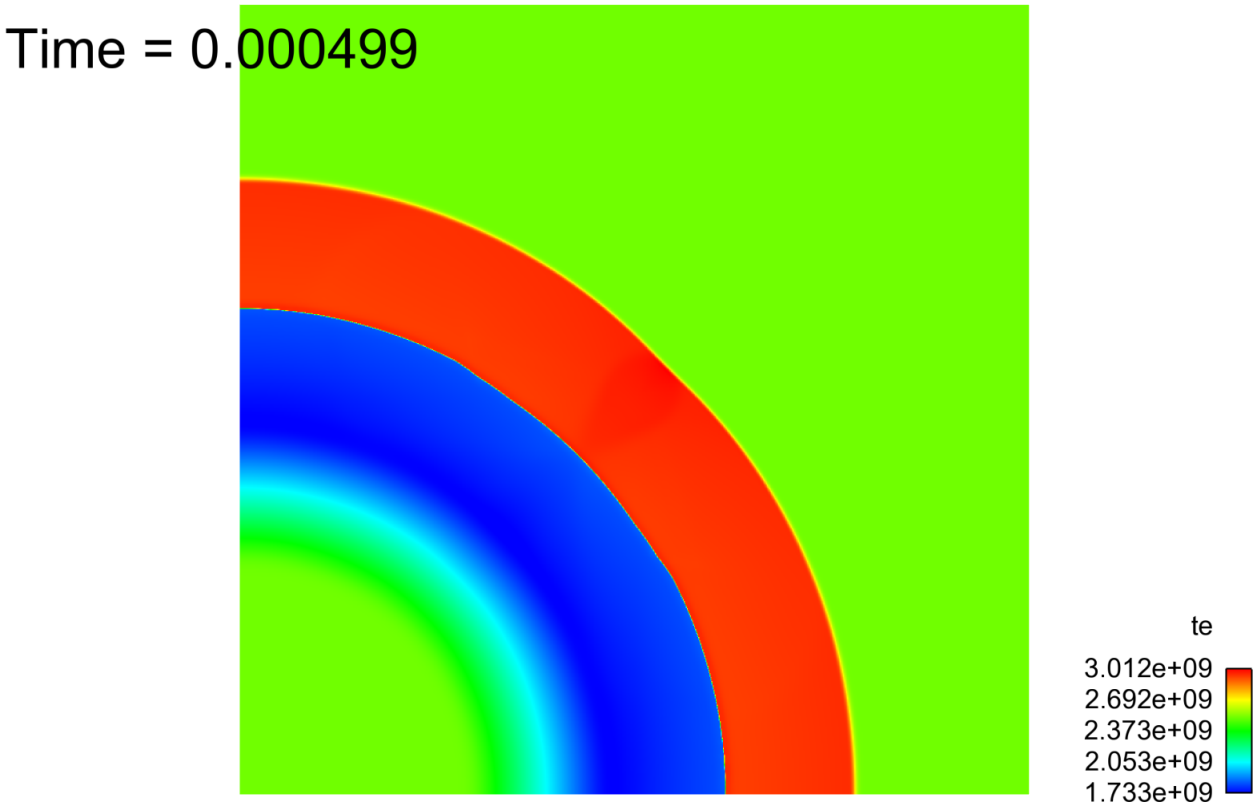

Figure 25: Implicit specific internal energy density.

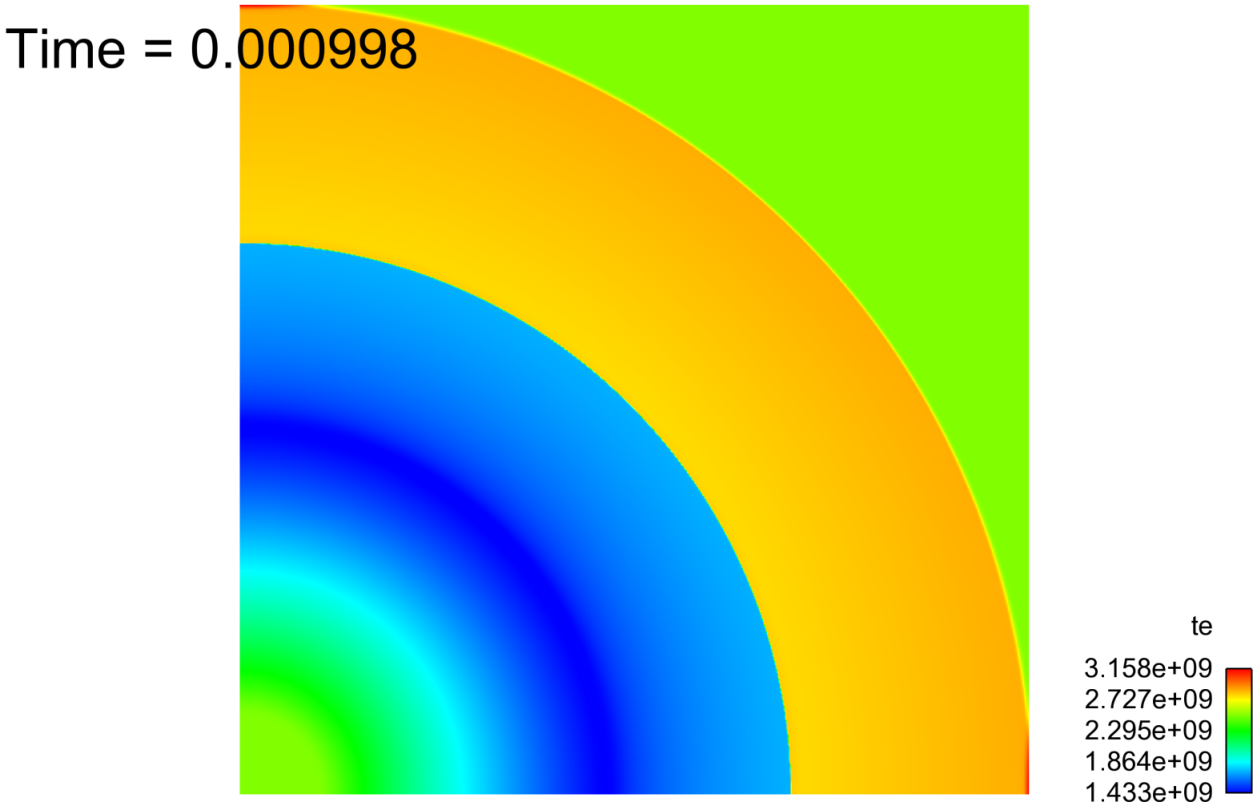

Figure 26: Explicit specific internal energy density.

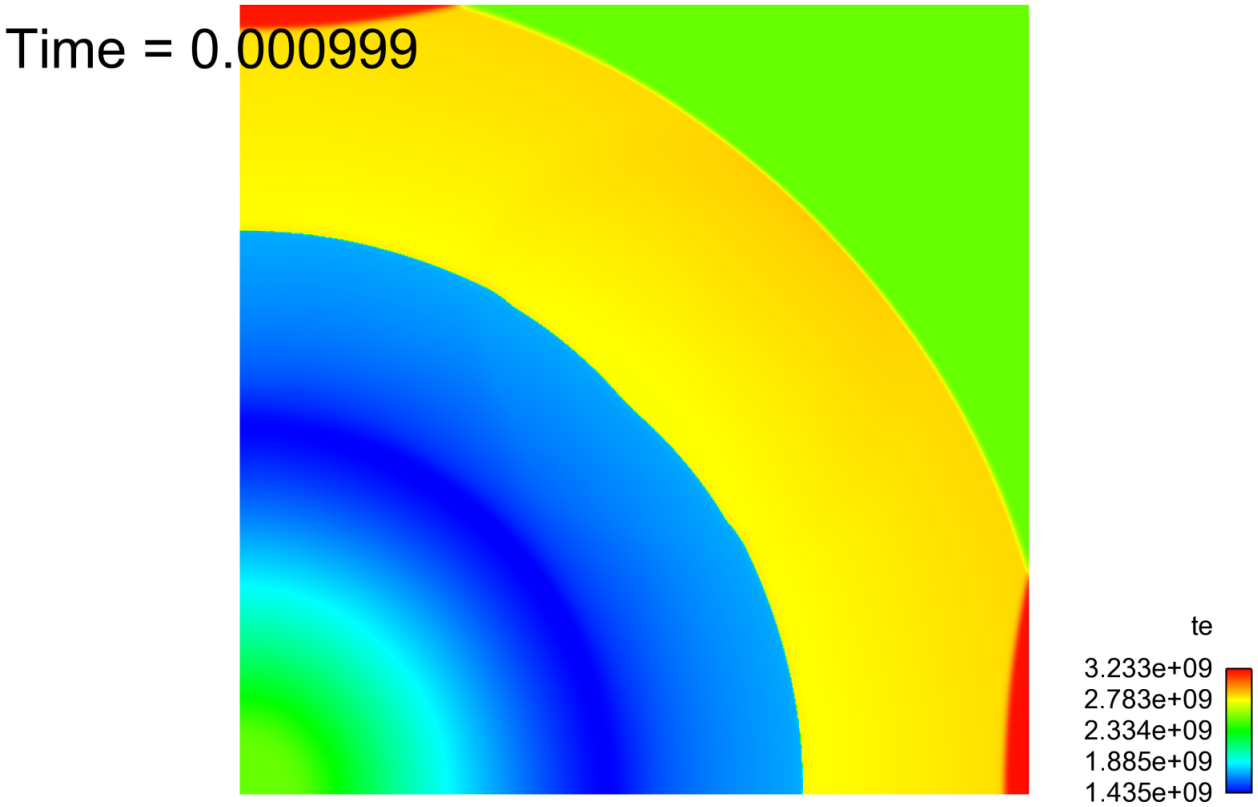

Figure 27: Implicit specific internal energy density.

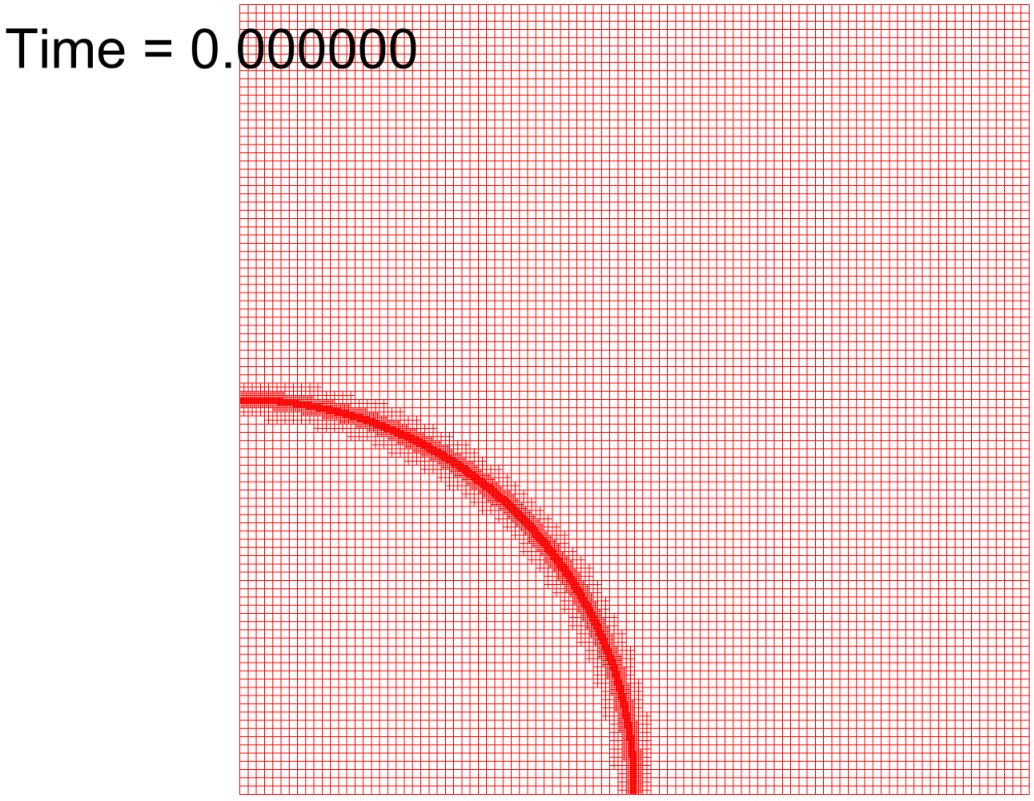

Figure 28: Implicit, 4-level, 16-processor mesh.

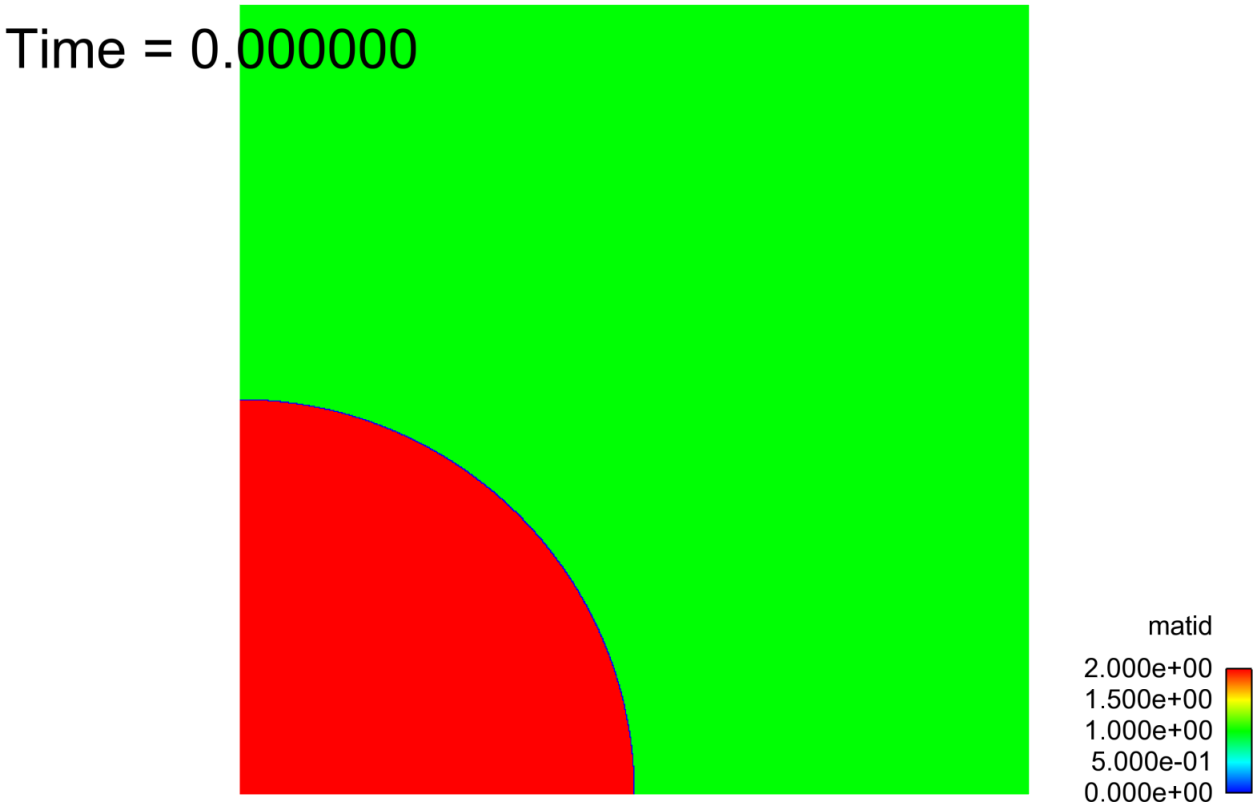

Figure 29: Implicit, 4-level, 16-processor material number.

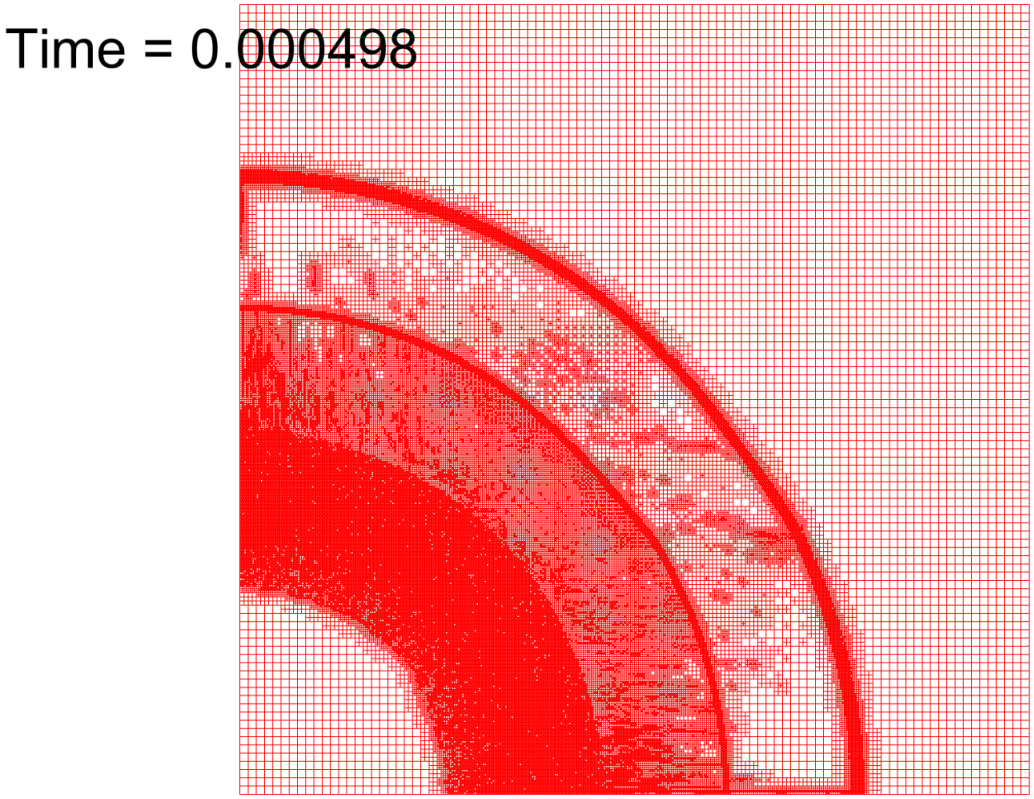

Figure 30: Implicit, 4-level, 16-processor mesh.

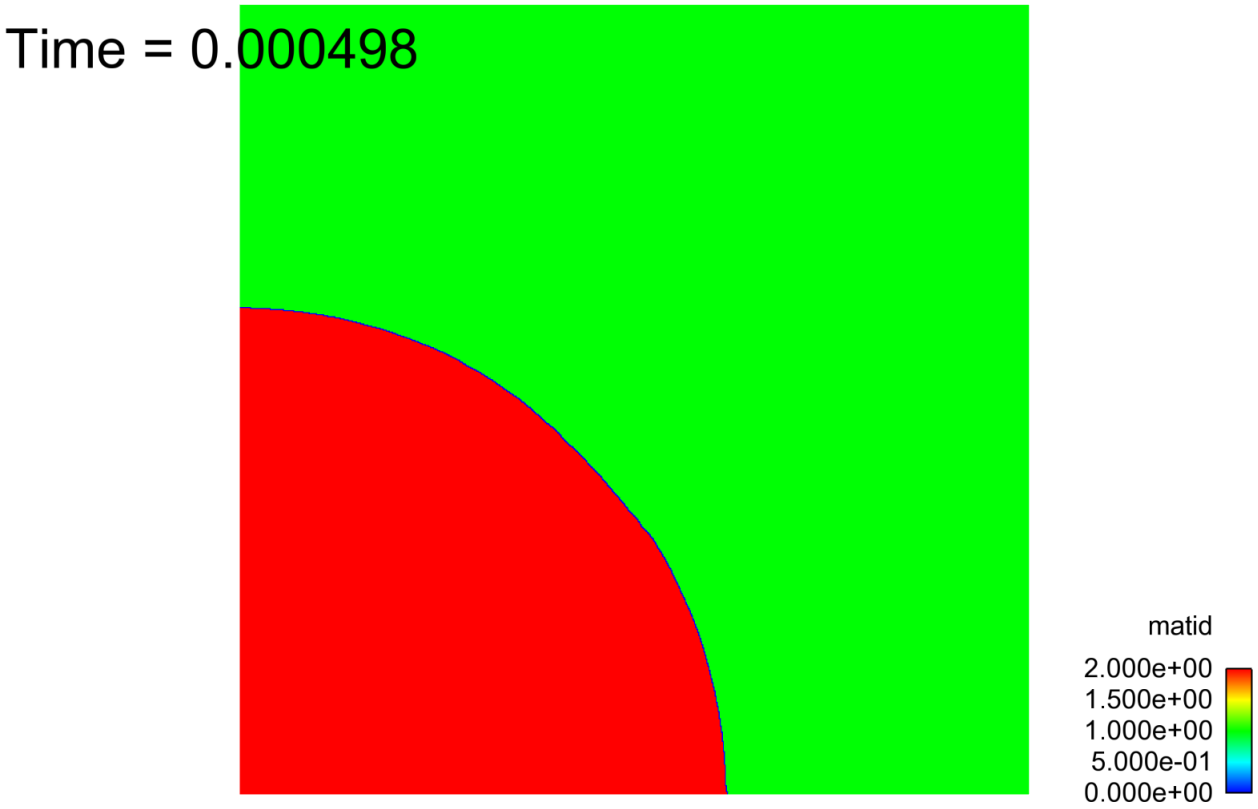

Figure 31: Implicit, 4-level, 16-processor material number.

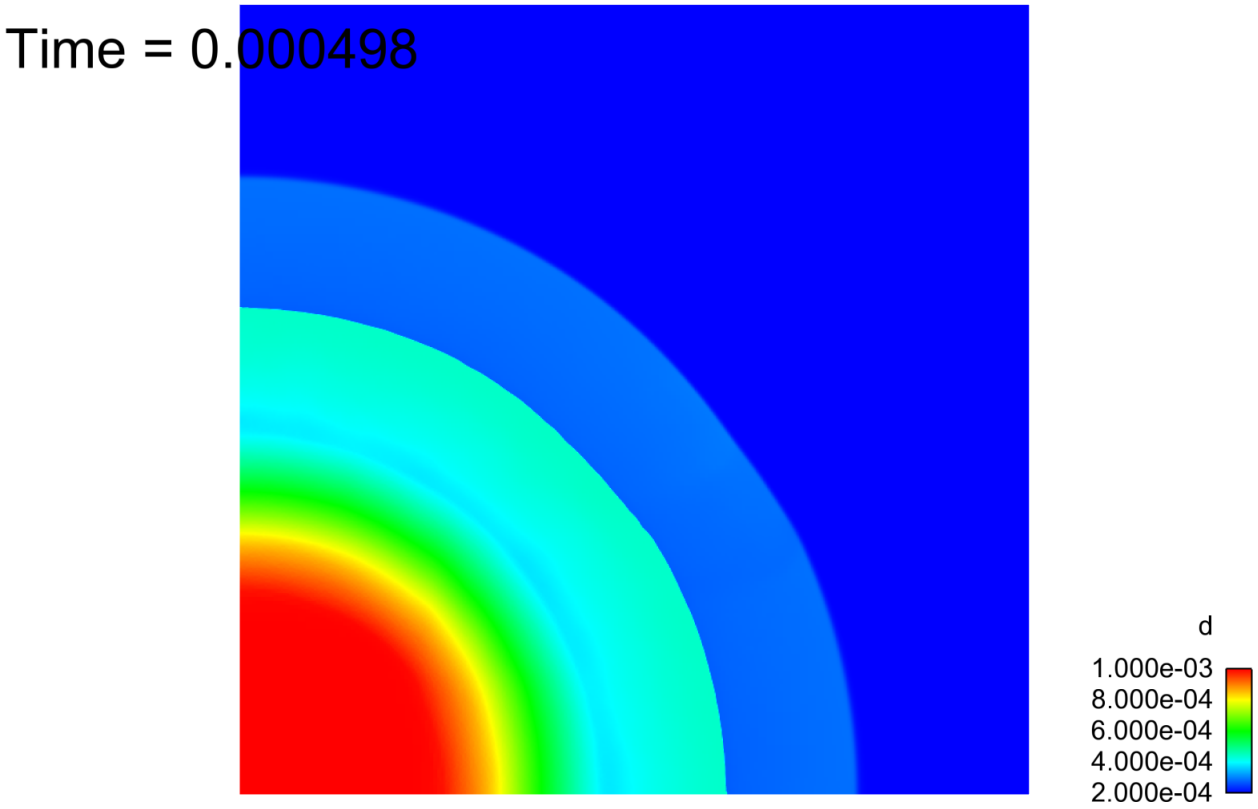

Figure 32: Implicit, 4-level, 16-processor density.

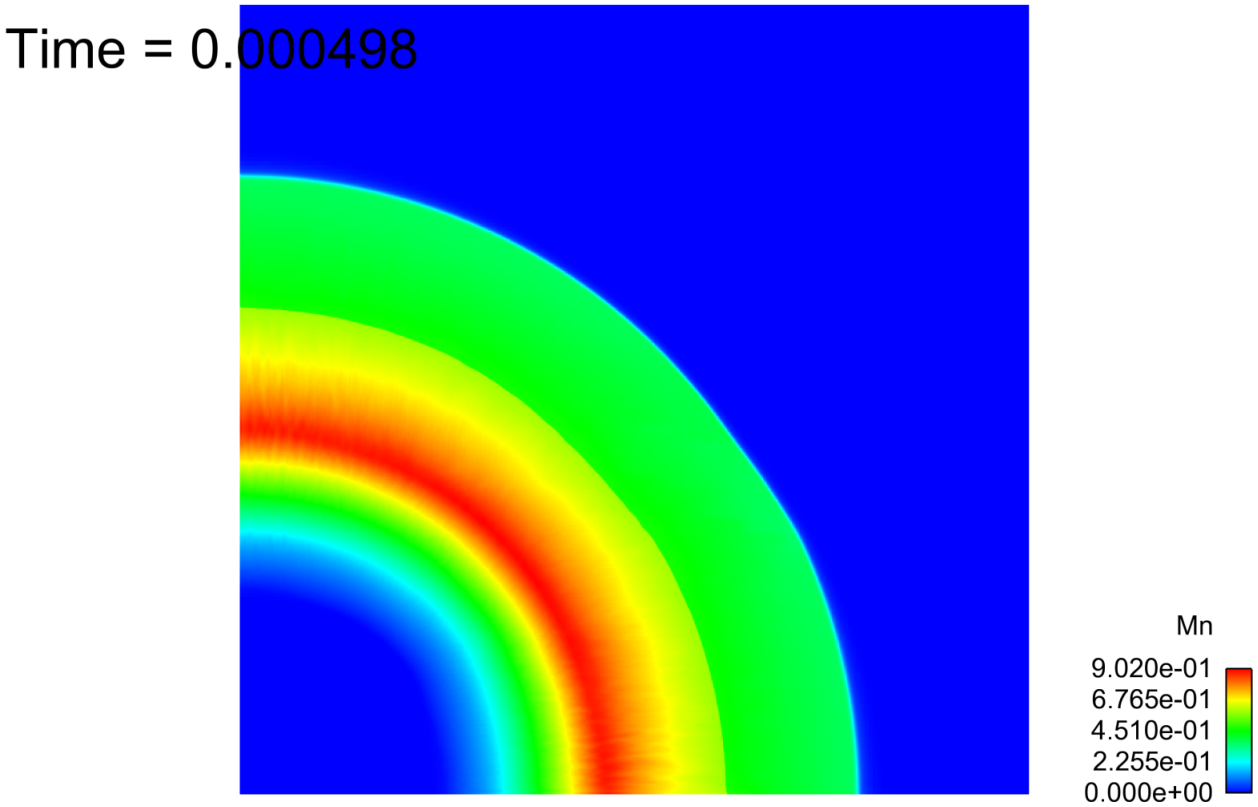

Figure 33: Implicit, 4-level, 16-processor Mach number.

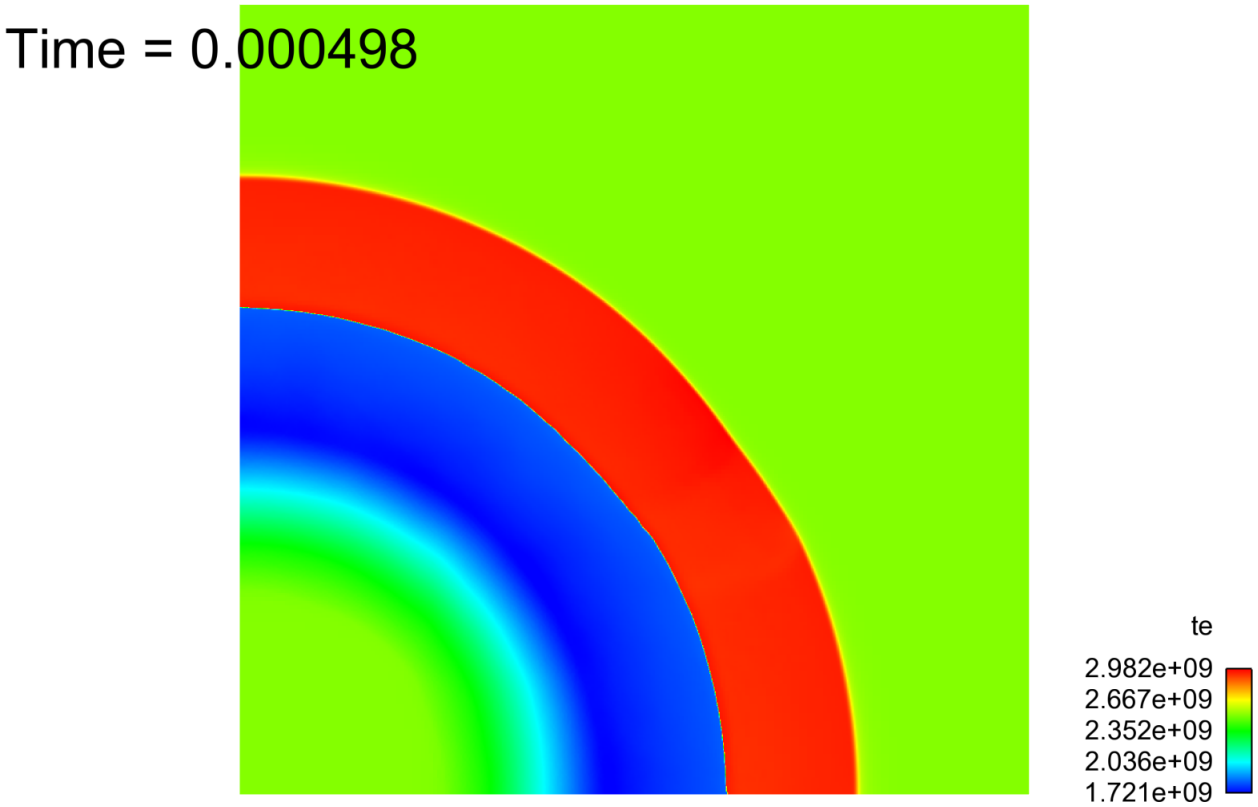

Figure 34: Implicit, 4-level, 16-processor specific internal energy.

6 Summary

Currently the parallel implicit hydrodynamics is modular, and runs in AMR with six possible geometries; 1-D planar/cylindrical/spherical, 2-D planar/cylindrical and 3-D planar. Both analytic and tabular Equations Of State are available in temperature and energy mode. No explicit Courant time step condition is required, however an accuracy time step control is used with the energy sources. In addition, implicit electron and ion thermal conduction, which is critical in Deflagration to Detonation Transition (DDT) simulations, is a part of the capability.

The next steps in the development of the parallel implicit hydrodynamics is to generalize to multi-pressure mixtures and extend the multi-species capabilities for low speed flow into the parallel implicit hydrodynamics, which will be compatible with the current multi-species velocity capability in the explicit hydrodynamics. This capability is needed, because species drift can occur in low speed flow and it has a longer time to evolve. Therefore, when the flow becomes shocked you have in place a mixture that was generated during the period of the low speed flow. Again, you cannot calculate with a Courant time step in the low speed regime.

The implicit hydrodynamics currently runs in the AMR code, BABBO, with mesh adaption, multi-phase advection, in both energy and temperature modes, and with viscous dissipation.

7 References

1. F. H. Harlow and A. A. Amsden, A Numerical Calculation Method for All Flow Speeds, J. Comp. Phys. 8 (1971), 197
2. A. Brandt, J. E. Dendy and H. Rupple, The Multigrid Method for Semi-Implicit Hydrodynamics Codes, J. Comp. Phys. 34 (1980), 348